Investigations on the Structure of Liquid Na-Cs Alloys

Huijben, M.J.; Lugt, W. van der; Reimert, W.A.M.; Hosson, J.Th.M. De; Dijk, C. van

Published in:
Physica B & C

DOI:
10.1016/0378-4363(79)90086-X

Publication date:
1979

Physica 97B (1979) 338–364

INVESTIGATIONS ON THE STRUCTURE OF LIQUID Na–Cs ALLOYS

M. J. HUIJBEN, W. VAN DER LUGT, W. A. M. REIMERT
Solid State Physics Laboratory, Materials Science Center, University of Groningen, Melkweg 1, 9718 EP Groningen, The Netherlands

J. Th. M. DE HOSSON
Department of Applied Physics, Materials Science Center, University of Groningen, Nyenborgh 18, 9747 AG Groningen, The Netherlands

and

C. VAN DIJK
Netherlands Energy Research Foundation ECN, 1755 LE Petten (N.H.), The Netherlands

Received 26 April 1979

The structure of liquid sodium–caesium alloys has been investigated for a large number of compositions covering the whole concentration range. X-ray as well as neutron diffraction techniques were employed. Special attention has been paid to the small-angle region of the diffraction pattern. The long-wavelength limit of the structure factor has been interpreted by applying a model proposed by Bhatia and March. Appreciable concentration fluctuations, indicating a tendency to phase separation, occur in the liquid. The size of the clusters was estimated using Guinier's model.

For a few concentrations, molecular dynamics computer simulations have been carried out. Different models for evaluating the three partial structure factors have been considered.

1. Introduction

The structure of a liquid, binary, alloy is described by three partial structure factors. As a consequence, three independent measurements are required for a complete analysis. In this paper dealing with sodium–caesium alloys we present experimental results obtained by X-ray and neutron diffraction, which in this context can be considered as providing independent information. As still a third source of information is needed, computer simulation experiments have been performed for a few compositions. Although altogether quite a number of data has been collected, the resulting picture is not entirely satisfactory as for none of the alloys a unique set of partial structure factors can be determined with sufficient accuracy. For this reason, not all of the experimental data will be communicated in this paper. A more comprehensive account has been given in the thesis of the first author. Readers interested in more details should direct themselves to the authors.

The sodium–caesium system is characterized by a large size difference of its constituent atoms: the atomic volume of caesium is three times that of sodium. Structural effects are anticipated. Indeed, the alloys system exhibits a considerable volume contraction on mixing [1]. Additionally, some other physical properties exhibit anomalies which possibly might be related to structural effects [2–5].

There exists no unique definition of the partial structure factors for a binary liquid. At the moment, in the literature three sets of such structure factors, mutually related by linear expressions, are coexisting. In this paper we will most frequently make use of the Ashcroft–Langreth (AL) structure factors S_{ij} defined by [6]:

$$S_{ij}(q) = N_i^{-\frac{1}{2}} N_j^{-\frac{1}{2}} \langle \rho_i^*(q)\, \rho_j(q) \rangle - N_i^{\frac{1}{2}} N_j^{\frac{1}{2}} \delta_{q,0}$$

$$= N_i^{\frac{1}{2}} N_j^{\frac{1}{2}} V^{-1} \int_V (g_{ij}(r) - 1) e^{-iq \cdot r} dr + \delta_{ij}. \quad (1.1)$$

Here $\rho_i(q) = \Sigma_{n=1}^{N_i} e^{iq \cdot R_n^i}$, R_n^i being the positions of atoms of species i, V is the total volume of the sample, N_i is the number of ions i and $g_{ij}(r)$ is a partial radial distribution function. In a liquid $S_{ij} = S_{ji}$.

Fluctuations in the total number $N = N_1 + N_2$ of atoms and in the composition are most easily dealt with using the Bhatia–Thornton (BT) structure factors $S_{NN}(q)$, $S_{CC}(q)$ and $S_{NC}(q)$. For their definitions, we refer to the original paper [7]. The relations between the BT structure factors and the thermostatistical properties of the binary liquid are given by

$$S_{CC}(0) = N\langle(\Delta C)^2\rangle = Nk_B T \Big/ \left(\frac{\partial^2 G}{\partial c^2}\right)_{p,T,N}, \quad (1.2a)$$

$$S_{NN}(0) = N^{-1}\langle(\Delta N)^2\rangle = \rho_0 k_B T \chi_T + \delta^2 S_{CC}(0), \quad (1.2b)$$

$$S_{NC}(0) = \langle \Delta N \Delta C\rangle = -\delta S_{CC}(0), \quad (1.2c)$$

where ΔN is the total number fluctuation in the volume considered and $\Delta C = N^{-1}(c_2 \Delta N_1 - c_1 \Delta N_2)$ is the composition fluctuation; c_i is the atomic fraction of component i, G is the Gibbs free energy of the system and

$$\delta = \left\{\left(\frac{\partial V}{\partial N_1}\right)_{T,p,N_2} - \left(\frac{\partial V}{\partial N_2}\right)_{T,p,N_1}\right\} \Big/ \left\{c\left(\frac{\partial V}{\partial N_1}\right)_{T,p,N_2} + (1-c)\left(\frac{\partial V}{\partial N_2}\right)_{T,p,N_1}\right\}. \quad (1.3)$$

Finally, for the interpretation of the data we will need the Faber–Ziman (FZ) partial structure factors $a_{ij}(q)$ [8]. They are rather similar to the AL structure factors but normalized such as to be independent of concentration in substitutional alloys. Their definition reads

$$a_{ij}(q) = 1 + (Nc_i c_j)^{-1}\langle \rho_i^*(q)\rho_j(q)\rangle - \delta_{ij} c_j^{-1} - N\delta_{q,0}$$

$$= 1 + \rho_0 \int_V \{g_{ij}(r) - 1\} e^{-iq \cdot r} dr, \quad (1.4)$$

where $\rho_0 = N/V$.

The total intensity diffracted by a binary system is

$$I(q) = \sum_{i=1}^{2}\sum_{j=1}^{2} f_i(q) f_j(q) \langle \rho_i^*(q)\rho_j(q)\rangle - N^2 \delta_{q,0} \quad (1.5)$$

which is a linear combination of the $S_{ij}(q)$; $f_1(q)$ and $f_2(q)$ are the atomic scattering factors. For a suitable presentation of the experimental data we introduce a "total interference function":

$$S(q) = \sum_{i=1}^{2}\sum_{j=1}^{2} c_i^{\frac{1}{2}} c_j^{\frac{1}{2}} \frac{f_i(q) f_j(q)}{\langle f^2(q)\rangle} S_{ij}(q), \quad (1.6)$$

where

$$\langle f^2(q)\rangle = c_1 f_1^2(q) + c_2 f_2^2(q). \quad (1.7)$$

The experimental details and the treatment of the raw data have been discussed elsewhere [9]. For the normalization, use has been made of the Warren–Krutter–Morningstar approximation [10] with satisfying results. The X-ray atomic scattering factors are adopted from Doyle and Turner [57] with dispersion corrections calculated by Cromer and Liberman [58], the neutron scattering cross sections were adopted from ref. 11. However, the neutron incoherent cross section for Cs was taken to be $\sigma = 0.095$ b, which is at variance with the value reported in ref. 11 (see ref. 9 for a justification of this choice).

The neutron measurements were carried out at two wavelengths: $\lambda = 2.58$ Å and $\lambda = 1.36$ Å, which permitted a larger range of wavenumbers to be investigated. The alkali metals were obtained commercially. The nominal purities are given as 99.93 at. % (Na) and 99.98 at. % (Cs).

The organization of the paper is as follows: In section 2 the experimental X-ray and neutron diffraction data will be presented. In section 3 particular attention will be paid to the small-wavenumber region of the diffraction patterns. In section 4 the computer simulation results will be presented and several models for interpreting the experimental data will be discussed.

2. Experimental results

Tables I and II list the compositions (indicated by the sodium concentration c_{Na}) and temperatures for which X-ray and neutron diffraction experiments have been performed. The majority of the total interference functions obtained are presented in the plots collected in fig. 1. We have omitted the plots representing the X-ray data for $c_{Na} = 0.1996, 0.4079, 0.6009, 0.6731$ and 0.8019, as well as the neutron data for $c_{Na} = 0.6008$, because they hardly provide any significant additional information.

The figures show that, with increasing sodium concentration, the oscillations in the diffraction pattern are progressively damped, but from $c_{Na} = 0.9$ (X-ray), resp. $c_{Na} = 0.7$ (neutron) onward the oscillation amplitude rises again. We also notice that, with increasing temperature, the peaks of the interference functions of all the alloys become lower and broader, whereas the positions of the peaks are independent of temperature.

Table I
Compositions and temperatures for which X-ray experiments have been performed

At % Na	Temperatures in °C			
10.01	43		100	150
19.96	30	65	100	
30.00	43		100	150
40.79		65	100	150
50.71		50	100	150
60.09		60	100	150
67.31		70	100	150
75.18		75	100	150
80.19		80	100	150
85.01		80	100	150
89.92		80	100	150
95.01			100	150
98.01			100	150

Table II
Compositions and temperatures for which neutron experiments have been performed

At % Na	Temperatures in °C		
0.00	30		
30.00	42	100	
50.75	50	100	
60.08	60	100	
75.17	75	100	
85.01	80	100	
89.92		100	
95.01		100	150
100.00		100	

For some concentrations about $c_{Na} = 0.85$ the structure factor, after passing through a minimum, increases again when q approaches zero. This proved to be an interesting phenomenon, some aspects of which have been discussed in a previous paper [12]. The effect is much more manifest in the neutron results than in the X-ray results, because the neutron measurements could be continued to smaller wavenumbers than the X-ray measurements. By suitable rearrangement of the experimental diffraction geometry, we were able to extend also the X-ray measurements to angles close to the central beam (which, admittedly, left us with an *upper* wavenumber limit for reliable experiments to be carried out). The "small-angle" X-ray results ($0.45° \leqslant 2\theta \leqslant 4°$) thus obtained were normalized by matching them to the higher angle results. Table III lists the compositions and temperatures for which small-angle experiments have been carried out and the graphs collected in fig. 2 give an impression of the matching procedure and the extrapolation to $q = 0$.

The smooth curve through the experimental points is obtained by using a spline function technique, which was present in the computer in the IMSL library [13]. The overall fit of the curves representing the larger angle scattering data to the small-angle scattering data is considered to be not entirely satisfactory, particularly not for the alloys containing 75 and 95 at. % sodium.

In fig. 3 the position q_m of the first X-ray peak is plotted as a function of the alloy composition. We observe a strong increase of q_m for $c_{Na} \geqslant 0.8$. The second, third etc. peaks of the total interference functions exhibit the same behaviour. In the neutron graphs this effect is less pronounced and takes place beyond $c_{Na} = 0.65$.

In fig. 4 the intensity of the X-ray main peak is plotted as a function of c_{Na} and, once more, a sudden rise for $c_{Na} \geqslant 0.9$ is found.

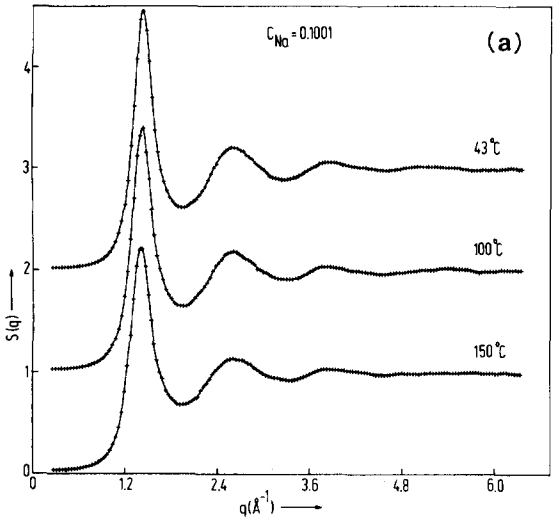
(a)
C_{Na} = 0.1001
43 °C
100 °C
150 °C
S(q)
q(Å^{-1})

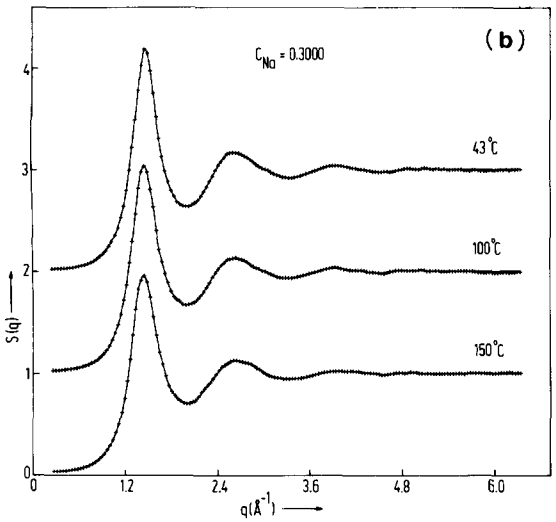
(b)
C_{Na} = 0.3000
43 °C
100 °C
150 °C
S(q)
q(Å^{-1})

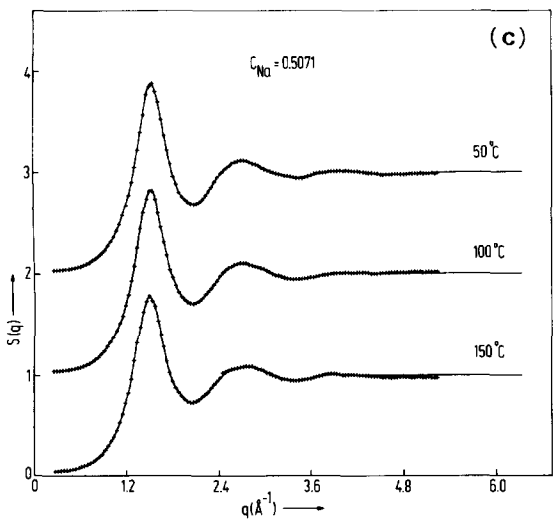
(c)
C_{Na} = 0.5071
50 °C
100 °C
150 °C
S(q)
q(Å^{-1})

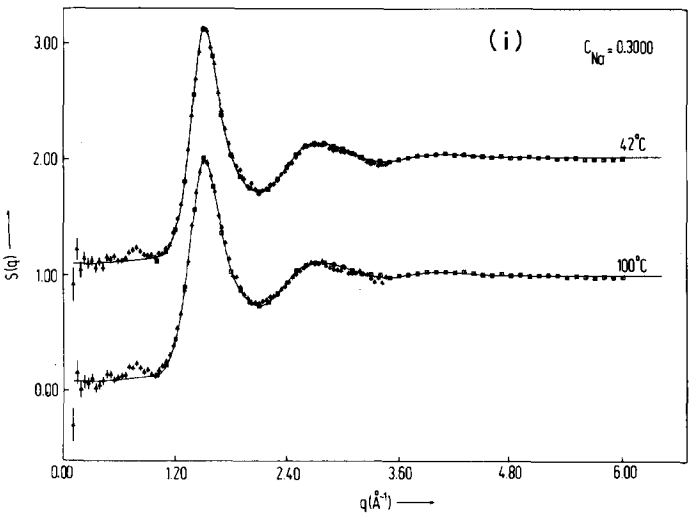
(i)
C_{Na} = 0.3000
42°C
100°C
S(q)
q(Å^{-1})

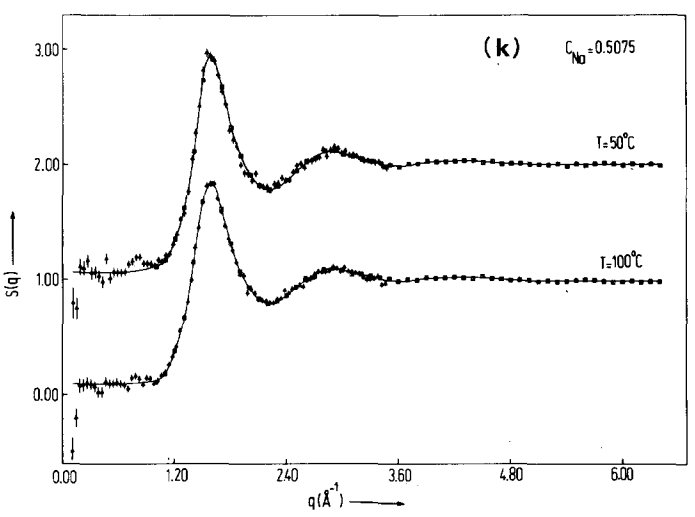
(k)
C_{Na} = 0.5075
T=50°C
T=100°C
S(q)
q(Å^{-1})

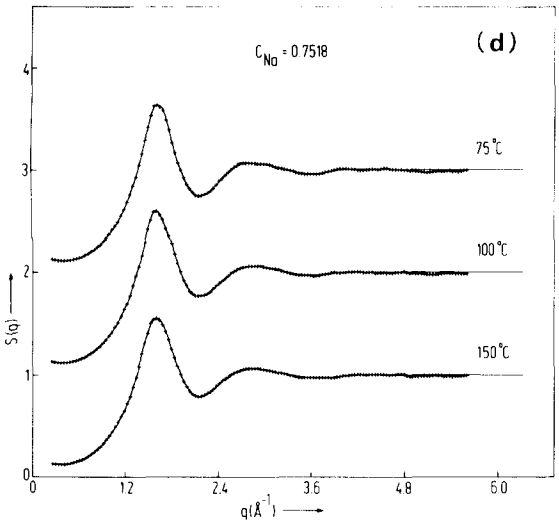
(d)
C_{Na} = 0.7518
75°C
100°C
150°C
S(q)
q(Å^{-1})

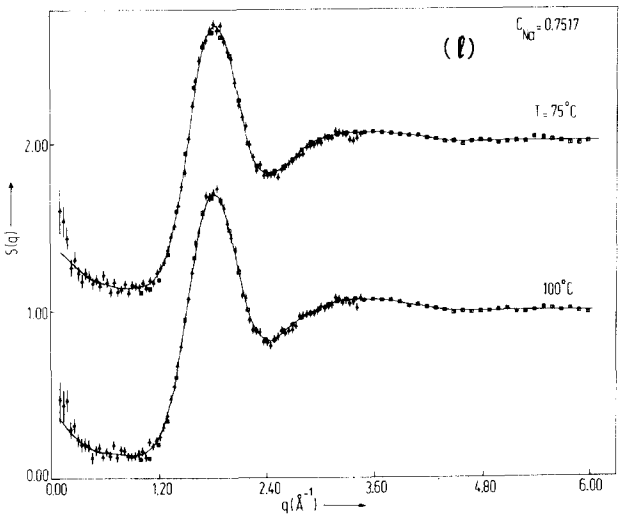
(ℓ)
C_{Na} = 0.7517
T = 75°C
100°C
S(q)
q(Å^{-1})

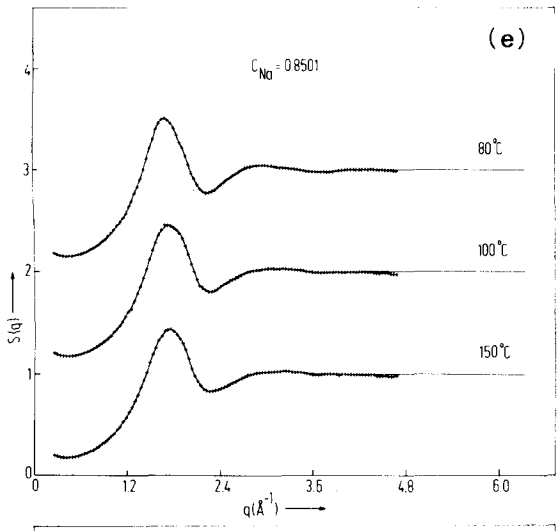
(e)
C_{Na} = 0.8501
80°C
100°C
150°C
S(q)
q(Å^{-1})

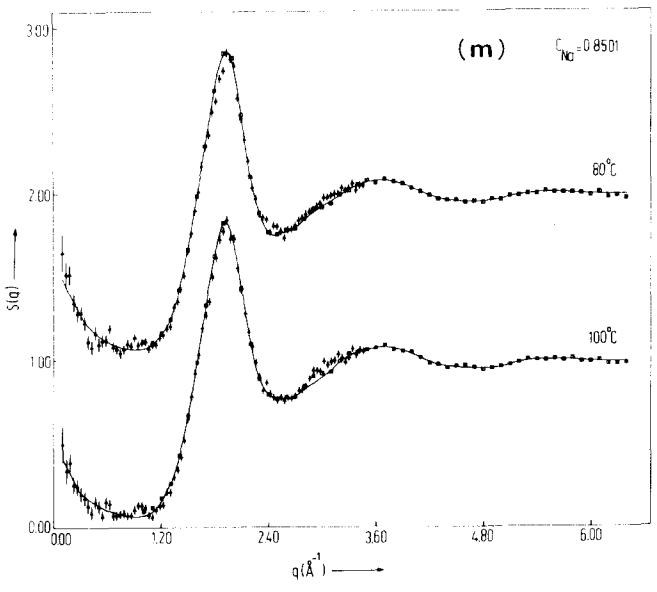
(m)
C_{Na} = 0.8501
80°C
100°C
S(q)
q(Å^{-1})

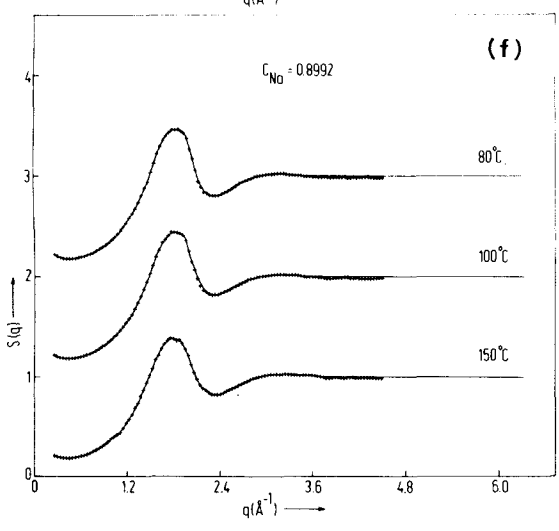
(f)
C_{Na} = 0.8992
80°C
100°C
150°C
S(q)
q(Å^{-1})

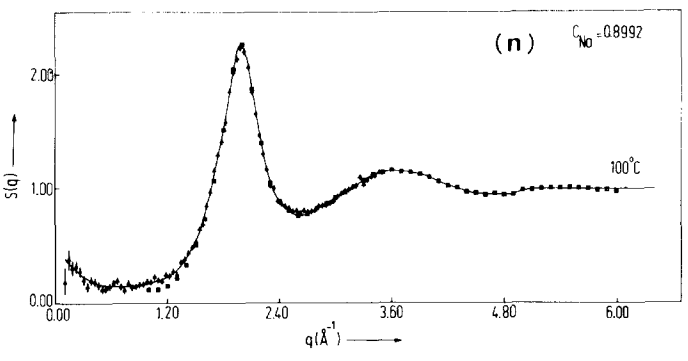
(n)
C_{Na} = 0.8992
100°C
S(q)
q(Å^{-1})

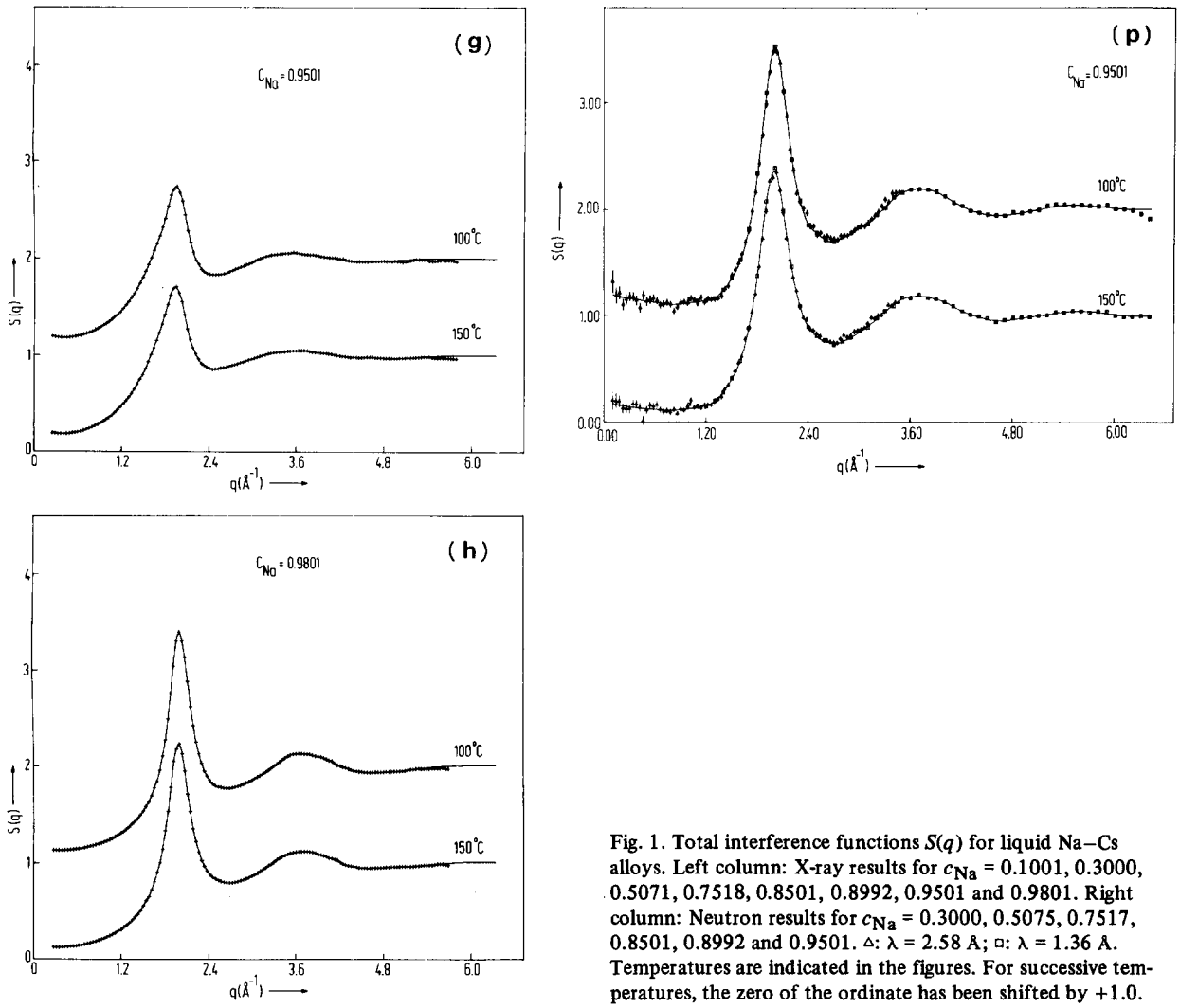

Fig. 1. Total interference functions $S(q)$ for liquid Na–Cs alloys. Left column: X-ray results for c_{Na} = 0.1001, 0.3000, 0.5071, 0.7518, 0.8501, 0.8992, 0.9501 and 0.9801. Right column: Neutron results for c_{Na} = 0.3000, 0.5075, 0.7517, 0.8501, 0.8992 and 0.9501. △: λ = 2.58 Å; □: λ = 1.36 Å. Temperatures are indicated in the figures. For successive temperatures, the zero of the ordinate has been shifted by +1.0.

Table III
Compositions and temperatures for which small-angle experiments have been performed

At % Na	Temperatures in °C	
75.19	75	100
80.22	80	100
85.01	80	100
89.93	80	100
95.01	100	150
98.01	100	

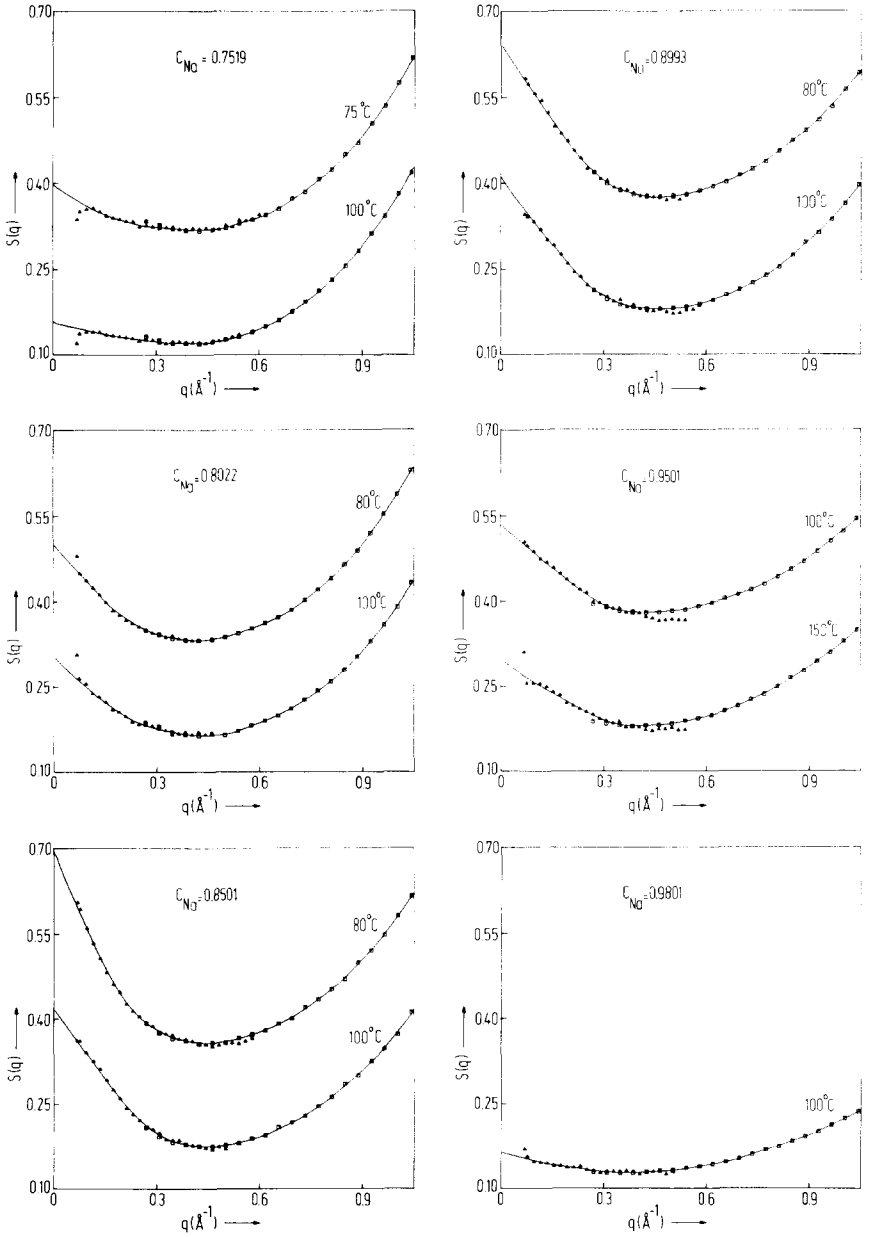

Fig. 2. Small-angle part of the X-ray total interference function $S(q)$ for compositions and temperatures indicated in the figures. △: small-angle measurements; □: larger-angle measurements. Values for $q < 0.07$ Å^{-1} obtained by extrapolation. For successive temperatures the zero of the ordinate has been shifted by +0.2

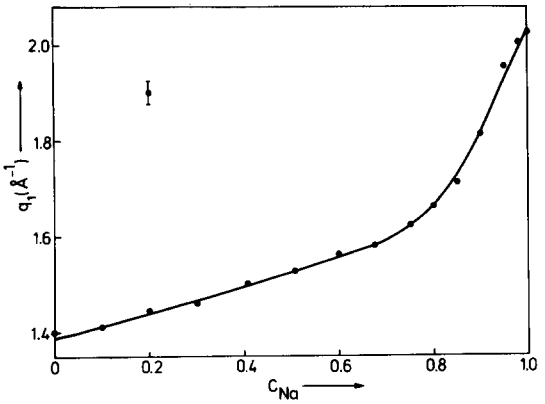

Fig. 3. Position of the main peak of the X-ray total interference function $S(q)$, plotted as a function of the sodium concentration, c_{Na}.

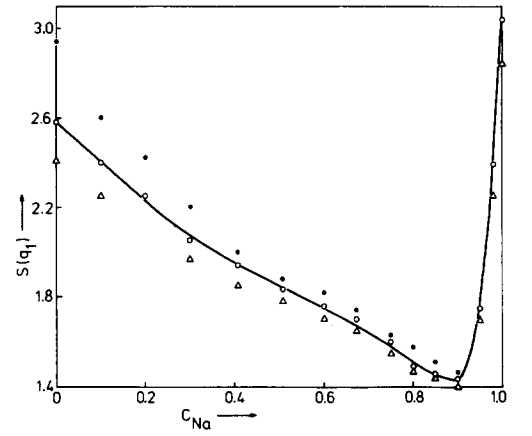

Fig. 4. Height of the main peak of the X-ray total interference function $S(q)$, plotted as a function of the sodium concentration, c_{Na}; Δ: T = 150°C; ○: T = 100°C; •: T either close to the melting point or, whenever the alloy is liquid at room temperature, 22°C.

3. Discussion of the small-q region of $S(q)$

The discussion in this section is divided into two parts. First, we will deal with the long-wavelength limit $S(0)$ of the total interference function. Secondly the Guinier model [14] will be applied to those results for which $dS(q)/dq$ is distinctly negative for small values of q.

3.1. Calculation of $S(0)$

The behaviour of $S(0)$ has already been briefly discussed in a previous paper [12]. Here, we mainly restrict ourselves to giving some additional comments.

Starting from the formulae (1.2a,b,c) the total interference function can be written as

$$S(0) = \frac{\langle f\rangle^2}{\langle f^2\rangle}\left[\left(\delta - \frac{f_1 - f_2}{\langle f\rangle}\right)^2 \cdot S_{CC}(0) + \rho_0 k_B T \chi_T\right], \tag{3.1}$$

where f_i is the scattering factor of atom i for $q = 0$. For calculating $S_{CC}(0)$ we use expressions given by Bhatia and March [15] which are based on a model for calculating the Gibbs free energy of mixing $\Delta_m G$ (cf. eq. (1.2a)):

$$S_{CC}(0) = c(1-c)/[1 - c(1-c)f(c)] \tag{3.2}$$

and

$$f(c) = [2\gamma^2 W - (\gamma-1)^2(\gamma - c(\gamma-1))]/[\gamma - c(\gamma-1)]^3, \tag{3.3}$$

where γ is the ratio of the molar volumes of the caesium and sodium atoms, and $W = w/k_B T$, w being the interchange energy. The expressions given by Bhatia and March are essentially based on statistical models for polymers formulated by Flory [16]. By means of eq. (1.3) we have calculated δ from earlier density determinations (Huijben et al. [1]). Consequently, the volume contraction occurring in the Na–Cs alloys system is taken into account.

Experimental values of the isothermal compressibility χ_T appearing in the term $\rho_0 k_B T \chi_T$ are not available for the Na–Cs alloys system, but χ_T is related to the adiabatic compressibility χ_s, which, in turn, can be derived from the results of sound velocity (v_s) measurements:

$$\chi_T = \frac{C_p}{C_V}\chi_s = \frac{C_p}{C_V}\cdot\frac{1}{\rho v_s^2}. \tag{3.4}$$

Here, C_p and C_V are the specific heats at constant pressure and volume. The sound velocities and the

densities have been measured by Kim and Letcher [4] and by Huijben et al. [1], respectively, but no experimental values of C_p/C_V are known for the alloys. As the values of C_p/C_V for sodium, potassium and caesium at 100°C are almost equal, it seems to be a reasonable guess to use this common value ($C_p/C_V = 1.13$) also for the alloys. Then it turns out, that the differences between the isothermal compressibilities derived in this way and those found by linear interpolation between the experimentally known values of χ_T for pure sodium and caesium are so small, that they can safely be neglected. Therefore, we finally have substituted in eq. 3.1 values of $\rho_0 k_B T \chi_T$ obtained by simple linear interpolation between the values of $S(0)$ for the pure metals.

In figs. 5 and 6 the theoretical values of $S(0)$ are shown as a function of the concentration c_{Na} for the X-ray diffraction and neutron diffraction case, respectively, together with the corresponding experimental values of $S(0)$. The quantity W appearing in the theory is adjusted such as to fit the theoretical results to the experimental values determined by the X-ray experiments. For $W = 1.04$ the experimental curve is in fair agreement with the theoretical curve. The peak in the theoretical curve is slightly shifted towards the caesium-rich side of the alloys system. The neutron data are also in reasonable agreement with the theoretical curve, though the scatter of the experimental points is much larger. The value of $W = w/k_B T$ pertains to $T = 100$°C.

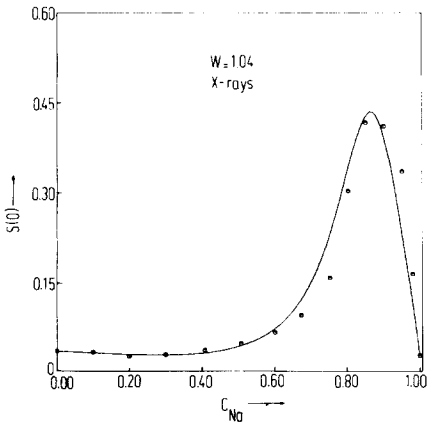

Fig. 5. $S(0)$ as obtained by X-ray diffraction, plotted as a function of the sodium concentration, c_{Na}. Curve: theoretical results; points: experiment. $W = w/k_B T$, with $T = 373$ K.

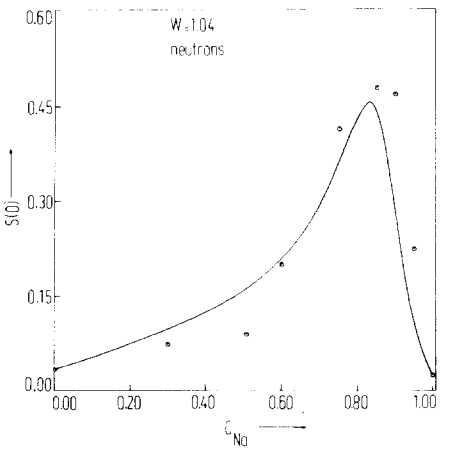

Fig. 6. $S(0)$ as obtained by neutron diffraction, plotted as a function of the sodium concentration, c_{Na}. Curve: theoretical results; points: experiment. $W = w/k_B T$, with $T = 373$ K.

The experimental error in the extrapolated X-ray diffraction intensities is estimated to be ±10%. This error is caused by counting errors, fitting the small-angle curve to the large-angle one and the extrapolation to $q = 0$. The experimental error in the extrapolated neutron diffraction data is estimated to be ±20% due to the larger scatter in the small-angle part of the measured intensities.

Using eqs. (1.2b, c) we have calculated $S_{NN}(0)$ and $S_{NC}(0)$ from $S_{CC}(0)$. The results are shown in fig. 7.

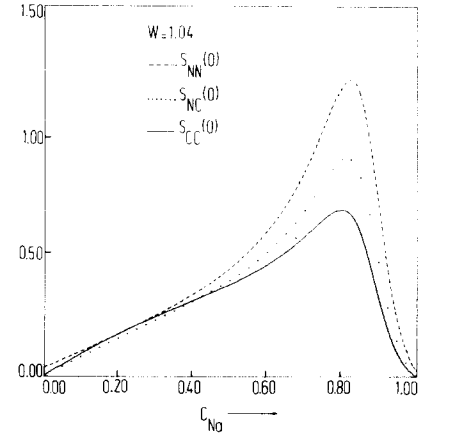

Fig. 7. Theoretical Bhatia–Thornton structure factors $S_{NN}(0)$, $S_{NC}(0)$ and $S_{CC}(0)$, plotted as a function of the sodium concentration, c_{Na}.

As a consequence of the relations between the BT partial structure factors at $q = 0$, the three curves look rather similar. The maximum in the curves is found at 80 at. % sodium.

The peak height of the $S_{CC}(0)$ versus c_{Na} curve is extremely sensitive to changes in W. E.g., when W is changed from 1.04 to 1.09, $S_{CC}(0)$ changes from 0.68 to 0.88. More generally, an increase in W produces a more pronounced peak.

The sign of W is important in discriminating between either compound forming or concentration fluctuations to occur: a negative value of W corresponds to compound formation, a positive value to concentration fluctuations in the liquid mixture. As a rule of thumb, the sign of W is in the following way reflected in the curve for $S_{CC}(0)$ vs. c_{Na}: a negative sign of W leads to a curve which does not exceed the "ideal" curve ($S_{CC}(0) = c(1-c)$), a positive sign of W corresponds to a curve with a pronounced peak. Deviations from this rule may originate from the contribution of the entropy to the free energy.

So, we may conclude, that we have found experimental evidence for concentration fluctuations to occur in liquid Na–Cs alloys in the vicinity of 80 at. % Na. This effect can be interpreted as a tendency to phase separation. It should be noted that the peak in $S_{CC}(0)$ in the Na–Cs system is less pronounced than it is, e.g. in the Tl–Te system [5], which exhibits a miscibility gap.

The parameter W can also be determined from other experiments. We mention here two properties in which W is involved.

3.1.1. Enthalpy of mixing

By reaction calorimetry, Yokokawa and Kleppa [17] have measured the enthalpies of mixing of sodium–caesium alloys at 111°C. They obtained positive enthalpies of mixing which, plotted as a function of composition, appear to be asymmetric with respect to $c_{Na} = 0.5$.

Making use of the same assumptions as for the calculation of $\Delta_m G$ [15] we obtain the following expression for the enthalpy of mixing (see also McClelland [18]):

$$\Delta_m E = \frac{\gamma c(1-c)}{c + \gamma(1-c)} Nw. \qquad (3.5)$$

From the experimental data for ΔE, $W = w/k_B T$ can be calculated. Then, W proves to be slightly dependent on the sodium concentration. But assuming $W = 0.77$ in eq. (3.5) at all compositions leads to a fair description of the asymmetric curve of the enthalpy of mixing (see fig. 8).

There exists a rather large discrepancy between this value for W and the value obtained from our experiments ($W = 1.04$). When $W = 0.77$ is substituted in the formula for $S(0)$ (eq. (3.1)) the maximum in the $S(0)$ versus concentration curve is reduced to 0.21. A substitution of $W = 1.04$ in $\Delta_m E$ (eq. (3.5)) yields a maximum of 317 cal/mol in the energy of mixing.

3.1.2. Chemical potential measurements

$S_{CC}(0)$ can be determined from electrochemical voltage measurements by the following equation

$$S_{CC}(0) = -\frac{N_A k_B T}{F}(1-c)\left(\frac{\partial \epsilon}{\partial c}\right)_{p,T,N}^{-1}, \qquad (3.6)$$

where ϵ is the electrochemical voltage, F is the Faraday constant and N_A is Avogadro's number. Ichikawa et al. [5], using an electrochemical cell, determined the chemical potential. Their results were analyzed by Bhatia and March [15] using the same model due to Flory as mentioned before. They find optimum agreement between the theoretical and experimental $S_{CC}(0)$ by choosing $W = 1.14$, which is to be compared with the value $W = 1.04$ resulting from our measurements.

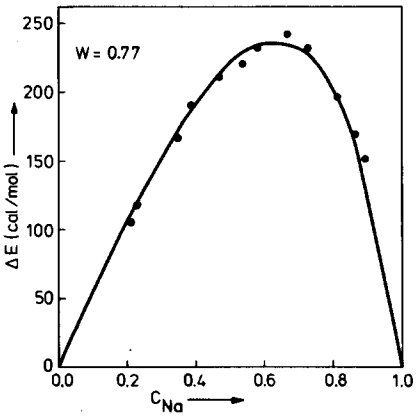

Fig. 8. Energy of mixing at 111°C of liquid Na–Cs alloys as a function of the sodium concentration. Points: experiments by Yokokawa and Kleppa [17]; curve: theory, eq. (3.5).

The significance of the agreement obtained is difficult to assess because of the extreme sensitivity of the expression (3.1) to the input data.

3.2. Guinier model

So far, our discussion has been restricted to the limit $q \to 0$. But the X-ray experiments show that the rise of $S(q)$, for decreasing, small, values of q, sets in already at $q \cong 0.4$ Å^{-1}. Evidently, this is due to the finite size of the fluctuations. Accordingly, the following discussion is based on the assumption that clusters of atoms, with a short lifetime, exist in the liquid. We will introduce a model developed originally by Guinier [14] for explaining the effect of homogeneous clusters in samples consisting of one component. The application of this model to binary liquid alloys, in which simultaneously different kinds of clusters may be present, constitutes an oversimplification of the state of affairs. Also, the assumption of Guinier, that the system be dilute, is not realized in our case. Nevertheless, the Guinier model has proved to be useful for obtaining rough estimates of the size of the clusters occurring in liquid alloys [20–22]. In the Guinier model the intensity scattered independently by all the clusters present in the mixture is given by

$$I(q) = C \cdot e^{-(1/3)q^2 R_g^2}, \tag{3.7}$$

where R_g is called the electronic radius of gyration of the cluster about its electronic center of mass and where C is a constant. Assuming that the clusters are spheres with radius R and homogeneously filled with electrons, one finds for R_g:

$$R_g^2 = \frac{3}{5} R^2, \tag{3.8}$$

and, consequently, for $I(q)$:

$$I(q) = C \cdot e^{-(1/5)q^2 R^2}. \tag{3.9}$$

The total intensity at small angles due to elastic scattering by the mixture can be separated into two parts. First, we have the contribution $S'(q)$ from the regions outside the clusters; it is approximately given by an extrapolation to small wavenumbers of the large angle scattering experiments (see, e.g., fig. 9). Secondly,

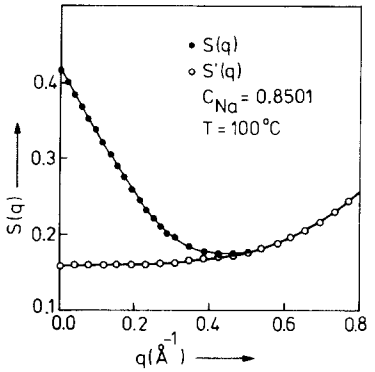

Fig. 9. Extrapolation of the larger-angle results, $S'(q)$, to small wavevectors for application in the Guinier model. Division of the interference function $S(q)$ in a "normal" part and a contribution from clusters. The alloy composition is $Na_{0.85}Cs_{0.15}$. ○: $S'(q)$; •: $S(q)$.

we find an intensity scattered by all the independent clusters in the mixture. Accordingly, the total intensity is given by:

$$I(q) = \langle f^2(q) \rangle S'(q) + C \cdot e^{-(1/5)q^2 R^2} \tag{3.10}$$

$$= \langle f^2(q) \rangle S(q). \tag{3.11}$$

Plotting ln $(\langle f^2(q) \rangle \cdot (S(q) - S'(q)))$ versus q^2 yields a straight line. The slope of this line determines the radius R of the cluster. As an example, in fig. 10, we have given this plot for an alloy at 100°C containing 85.01 at. % Na. The straight line in this figure is fitted to the points between $2\Theta = 0.625°$ and $2\Theta = 1.50°$, because for these scattering angles the measured

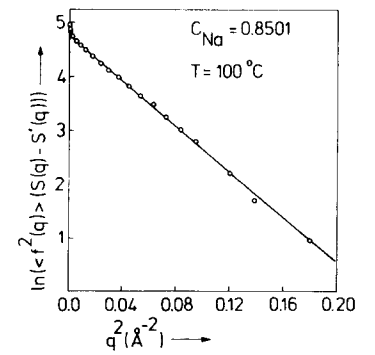

Fig. 10. Plot of ln $(\langle f^2(q) \rangle \cdot [S(q) - S'(q)])$ as a function of q^2 for determining the cluster radius.

intensities are most reliable and the intensity contribution from cluster scattering is still sufficiently large.

For each of the investigated alloys the radius of the cluster was determined from the slope of the lines. Only X-ray results have been considered. Fig. 11 shows the radius of the clusters versus the Na concentration. The radius of the cluster at a certain concentration is obtained as the average of the radii at different temperatures, assuming that the radius does not vary appreciably with temperature. We find that the radius R of the clusters is approximately 10.4 Å ± 0.5 Å. This number is fairly constant in the entire composition range of 80–98 at. % Na.

The results for $S(q)$ are shown in fig. 12. A discrepancy between the theoretical structure factor as calculated by eq. (3.10), neglecting the departures from the straight line in fig. 10, and the experimental $S(q)$ exists at small values of q. In our experimental data we did not find an indication for a flattening of the scattered intensity if q approaches zero. Also, the division of the total intensity in Guinier intensity and "normal" intensity is rather arbitrary.

We have to admit that this description of the small-angle scattering is not completely adequate. The Guinier method was applied with much better results to the Bi–Cu alloys system by Zaiss and Steeb [22]. The accuracy obtained by Hoehler and Steeb [21] in their treatment of Al–In alloys is comparable to ours.

Finally, it should be remarked that the radius of e.g. a Cs-atom (2.4 Å) is not extremely small compared with the observed cluster radius (≃10 Å). This questions the validity of the supposition of a homogeneous cloud of electrons, which lies at the basis of the Guinier method.

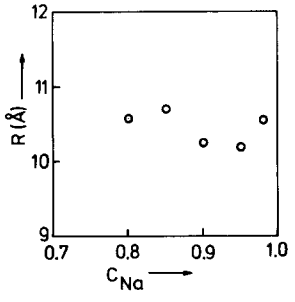

Fig. 11. Cluster radius R as a function of sodium concentration c_{Na}.

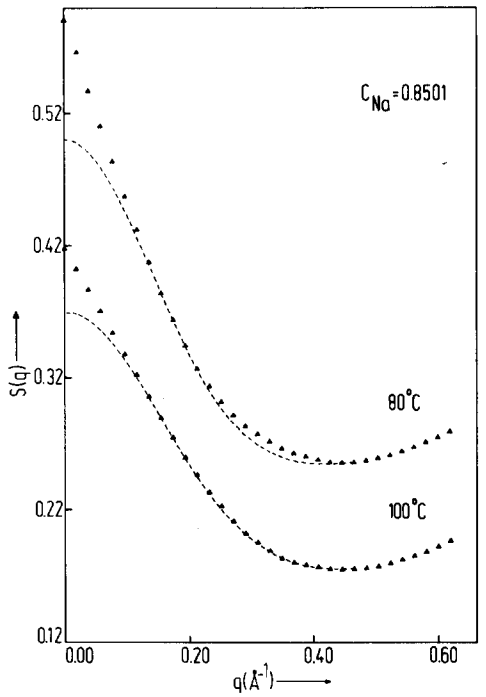

Fig. 12. – – – $S(q)$ according to Guinier model, neglecting the deviations from linearity of the curve in fig. 10. ▲ Experimental (and extrapolated) points. The zero of the ordinate of the 80° C curve is shifted upwards by +0.1.

In section 4 we will pay attention to a procedure for introducing long-range interactions in the expressions describing the structure factors for a binary system of hard spheres. It will be shown that particularly the small-angle region is affected by these interactions.

4. General analysis and computer experiments

In section 3 we have provided some theoretical approximations for describing the long-wavelength limit and the small-q part of the total interference function. The aim of this section is to give an impression of the difficulties arising in the determination of a unique set of partial structure factors for the entire range of wavevectors q. The two different experiments are insufficient to obtain these three independent partial structure factors. Therefore, we have to introduce theoretical models to solve this problem. The most substantial additional information is derived

from computer experiments, which, as a consequence of limited computer time, could be performed for only two of the compositions.

From the partial structure factors, thus obtained, the total interference functions for X-ray as well as neutron diffraction are constructed and compared with experiment. One of the models introduced can be extended to include the small-wavenumber range and constitutes a useful supplement to the discussion in the preceding section. At the end of this section we discuss, for a few selected compositions, the models which are, to our opinion, most suitable for describing the partial structure factors. All total interference functions, discussed in this section, pertain to $T = 100°C$.

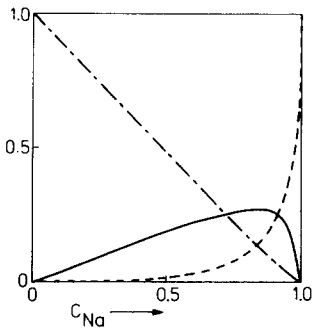

Fig. 13. Coefficients $c_i c_j f_i(q) f_j(q)/\langle f^2(q)\rangle$ at $q = 1.71$ Å^{-1} as a function of the sodium concentration c_{Na}. The $f_i(q)$ pertain to scattering of X-rays. The coefficients appear to be constant in the range 1.40 Å$^{-1} < q < 2.02$ Å^{-1}. – – – – i = Na, j = Na; – · – · – i = Cs, j = Cs; ——— i = Na, j = Cs.

4.1. Composition-independent FZ partial structure factors

In section 1 we have noticed that, in substitutional alloys, the FZ partial structure factors $a_{ij}(q)$ are independent of composition. Extending this property to non-substitutional alloys is an obvious approximation, which has been applied by a number of authors [23–32]. Although the Na–Cs system is distinctly non-substitutional, this approach still seems to be justified by the following observations.

Let us apply the assumption of composition-independent FZ structure factors to the sodium–caesium system. We expect that, at the value of q corresponding to the main peak in the structure factor for pure caesium ($q = 1.40$ Å^{-1}), a_{CsCs} will provide the dominant contribution to the total interference function $S(q)$. Then, we see from eqs. (1.1), (1.4) and (1.6) that, at $q = 1.40$ Å^{-1}, the composition dependence of $S(q)$ should follow closely that of the coefficient $c_{Cs}^2 f_{Cs}^2(q)/\langle f^2(q)\rangle$. The same kind of correspondence should exist between the composition dependence of $S(q)$ at $q = 2.02$ Å^{-1} (the position of the main peak for pure sodium) and $c_{Na}^2 f_{Na}^2(q)/\langle f^2(q)\rangle$. We may further extend these arguments to the main peak of a_{NaCs}: since at none of the compositions any splitting of the first peak of $S(q)$ has been observed, it is reasonable to suppose that $a_{NaCs}(q)$ has its main maximum at a position approximately halfway between those of a_{NaNa} and a_{CsCs}, i.e. at 1.71 Å^{-1}.

Indeed, a comparison of figs. 13 and 14, pertaining to the X-ray measurements, shows that the supposed

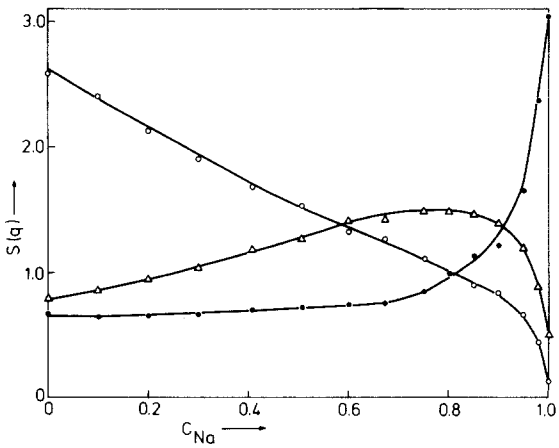

Fig. 14. X-ray experimental structure factors, at selected values of q, as a function of the sodium concentration c_{Na}. ○: $q = 1.40$ Å^{-1}; △: $q = 1.71$ Å^{-1}; •: = $q = 2.02$ Å^{-1}.

qualitative correspondence exists. The same observations have been made with respect to the neutron experiments. The assumption of concentration independent FZ structure factors has been worked out in two different ways:

i) by choosing $a_{NaNa}(q)$ and $a_{CsCs}(q)$ equal to the structure factors $S_{Na}(q)$ and $S_{Cs}(q)$ of the respective pure metals;

ii) by deriving the FZ structure factors from experimental intensities at three different concentrations of the alloys system.

i) Starting with the first method, we may write down the total interference function in terms of

$S_{Na}(q)$, $S_{Cs}(q)$ and $a_{NaCs}(q)$:

$$S(q) = \frac{\langle f^2(q)\rangle - \langle f(q)\rangle^2}{\langle f^2(q)\rangle} + c_{Na}^2 \frac{f_{Na}^2(q)}{\langle f^2(q)\rangle} S_{Na}(q) + c_{Cs}^2 \frac{f_{Cs}^2(q)}{\langle f^2(q)\rangle} S_{Cs}(q) + 2c_{Na}c_{Cs} \frac{f_{Na}(q) f_{Cs}(q)}{\langle f^2(q)\rangle} a_{NaCs}(q) \qquad (4.1)$$

and, next, calculate $a_{NaCs}(q)$ from eq. (4.1) for different compositions and see whether or not the results are compatible. This procedure was carried out for compositions at which the contribution of $a_{NaCs}(q)$ to the total intensity is largest, i.e. at 80, 85 and 90 at % Na for the X-ray experiments and 50, 60 and 75 at % Na for the neutron experiments. The results, particularly those for the X-ray case, are encouraging (figs. 15 and 16). The wiggle in front of the main peak is presumably due to the strong q-dependence of $S_{Cs}(q)$ at that position. Next, the partial structure factors $a_{NaCs}(q)$, evaluated in this way, are combined with $S_{Na}(q)$ and $S_{Cs}(q)$ to reconstruct $S(q)$ at several compositions differing from those from which the $a_{NaCs}(q)$ were derived. The results are shown in figs. 17 and 18. Depending on the composition and the kind of experiment considered, the results vary from satisfactory to disappointing.

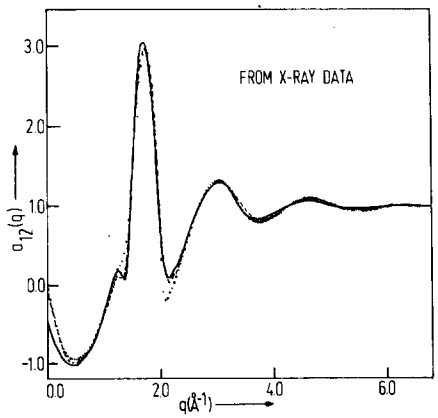

Fig. 15. FZ partial structure factors $a_{NaCs}(q)$ derived from X-ray measurements of $S(q)$ using the assumption of concentration-independent FZ structure factors. ——— 80.19 at. % Na, – – – – – 85.01 at. % Na, · · · · · 89.92 at. % Na.

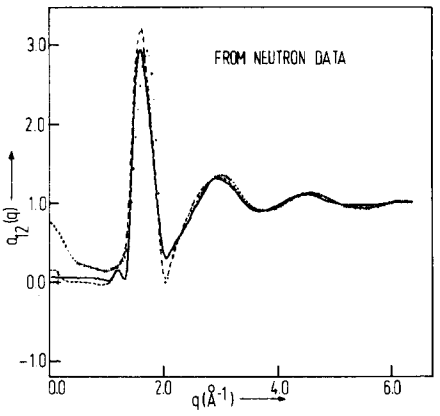

Fig. 16. FZ partial structure factors $a_{NaCs}(q)$ derived from neutron diffraction measurements of $S(q)$ using the assumption of concentration-independent FZ structure factors. ——— 50.75 at. % Na, – – – – – 60.08 at. % Na, · · · · · 75.17 at. % Na.

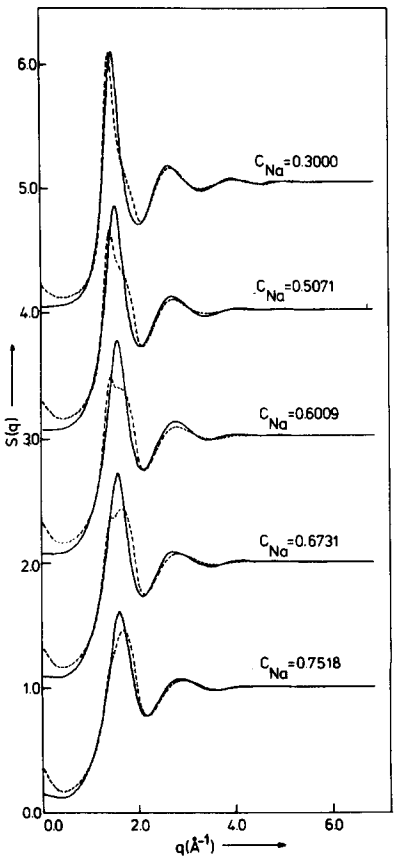

Fig. 17. X-ray total interference functions $S(q)$ (for several compositions indicated in the figure) according to the assumption of concentration-independent FZ structure factors. ——— experiment; – – – – – theory.

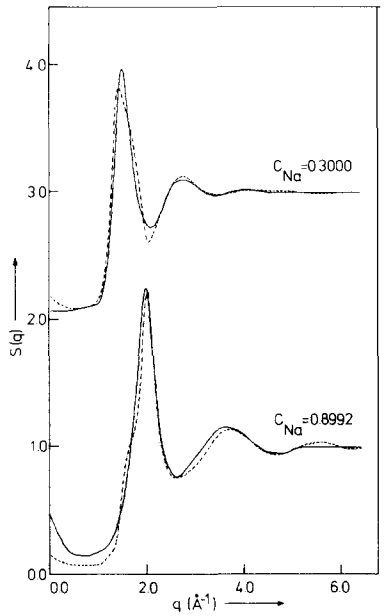

Fig. 18. Neutron total interference functions $S(q)$ for two compositions indicated in the figure, according to the assumption of concentration-independent FZ structure factors. ——— experiment; – – – – – theory.

ii) The second procedure has also been explored but proves to lead to strongly inconsistent results. We share this conclusion with Korsunsky and Naberukhin [33]; the reader is referred to their paper for a detailed criticism of this procedure. Summing up, we conclude that the method of concentration-independent FZ partial structure factors, although promising in some respects, doesn't come up to the expectations.

4.2. Hard-sphere solution of the Percus–Yevick equation

The most commonly used theoretical approach to the calculation of structure factors, are the analytical solutions of the Percus–Yevick equation for hard-sphere potentials (HSPY). For binary systems, they have been derived by Lebowitz [34]. As input parameters one needs to specify the hard sphere diameters d_1 and d_2 and the packing fraction η. Although the HSPY structure factors describe the general shape of the structure factors rather well, it usually is not possible to find a quantitatively satisfactory fit simultaneously in the small-angle region (up to and including the main peak) and at larger angles. More particularly the oscillations beyond the first peak are often exaggerated [35]. Below we will display the results from the HSPY formulae in their original form as well as those from three modified versions.

4.2.1. HSPY-method with fixed η and d_i

For a straightforward application of the HSPY-theory, we have to decide upon a suitable set of parameters (η, d_1, d_2). We have assumed that all the parameters are independent of composition. For η we have chosen $\eta = 0.45$, which is a customary value in liquid metals. For the hard-sphere diameters we have adopted values from Hafner [36] and Ratti and Bhatia [37]: $d_{Na} = 3.15$ Å and $d_{Cs} = 4.80$ Å. The resulting HSPY total interference functions are shown in fig. 19 and fig. 20 and compared with the experimental results. The agreement between theory and experiment is satisfactory for values of q up to and including the main peak (except for $q \to 0$ at those concentrations for which appreciable composition fluctuations occur), but, as expected, the oscillations at larger values of q are much too strong.

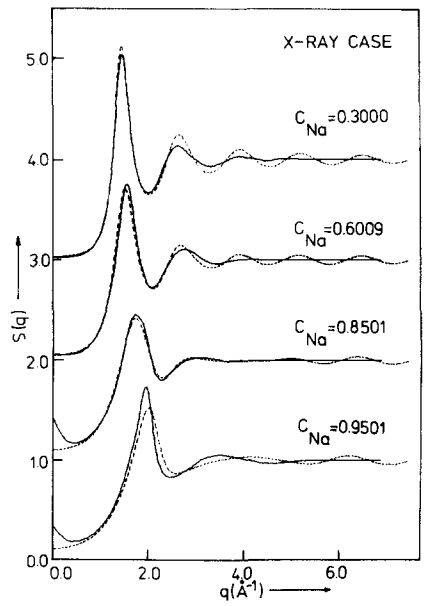

Fig. 19. HSPY (fixed η, d_i) values for $S(q)$ (– – – – –) compared with X-ray diffraction results (———).

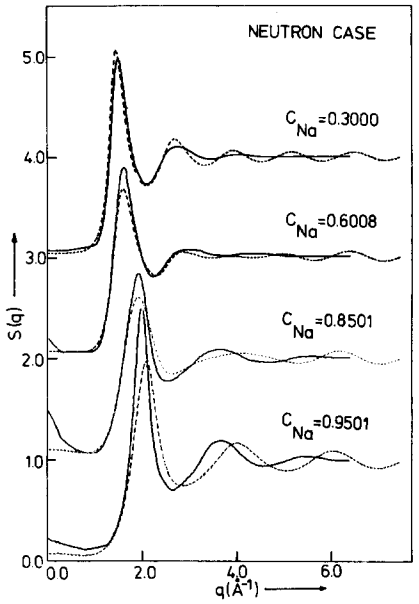

Fig. 20. HSPY (fixed η, d_i) values for $S(q)$ (– – – – –) compared with neutron diffraction results (———).

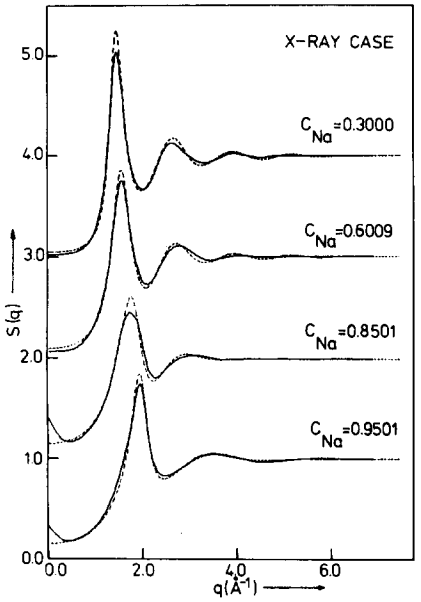

Fig. 21. HSPY (variable,η, d_i) values for $S(q)$ (– – – – –) compared with X-ray diffraction results (———).

4.2.2. *HSPY method with variable η and d_i*

A refinement can be obtained by introducing q-dependent d_i and η. The physical meaning of doing so is questionable, and this procedure should be considered mainly as a mathematical trick to find explicit expressions for the partial structure factors.

First, for pure Na and Cs, $\eta(q)$ and $d_i(q)$ are obtained by adjustment of the HSPY structure factor to the experimental one at a number of maxima and minima of $S(q)$. Between the maxima and minima the η and d_i are obtained by linear interpolation. For the binary mixture the packing fraction η is given by:

$$\eta(q) = c_{Na}\eta_{Na}(q) + c_{Cs}\eta_{Cs}(q). \qquad (4.2)$$

For a number of compositions the HSPY total interference function is compared with the experimental data obtained by X-ray diffraction (fig. 21) and by neutron diffraction (fig. 22). Reasonable overall agreement has been obtained. Comparing the results with those from the unmodified (fixed η, d_i) HSPY-method, we notice that the strong oscillations beyond the first peak are considerably reduced and the phase of the remaining oscillations is described much more correctly. Only in the region up to and including the first peak the unmodified version gives slightly better results.

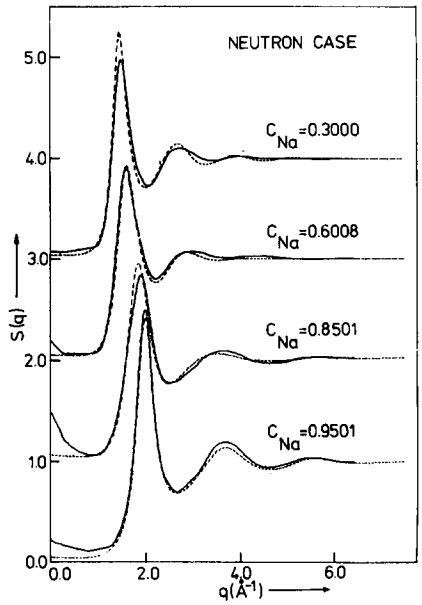

Fig. 22. HSPY (variable η, d_i) values for $S(q)$ (– – – – –) compared with neutron diffraction results (———).

From the figures we notice that neither of the two HSPY approaches is able to describe satisfactorily the

long-wavelength limit of $S(q)$ when strong concentration fluctuations are present in the liquid (at $c_{Na} \approx 0.85$).

4.2.3. Molecular aggregates

Furthermore, a model description developed by Bhatia and Ratti [38] has been explored. In this model, the liquid is supposed to contain molecular aggregates, called compound atoms by the authors. The compound atoms are made spherically symmetric and subsequently treated as being hard spheres with an effective scattering factor. Finally, HSPY theory is applied to the mixture of single atoms and compound atoms. Bhatia and Ratti obtained satisfactory results for the Li–Pb and Cu–Cl systems, which exhibit compound forming.

In the Na–Cs system no compound forming, but a tendency to phase separation occurs. We could easily adapt the Bhatia–Ratti procedure to this case. The tendency to phase separation is accounted for by constructing compound atoms out of one of the components and treating the atoms of the other component as single particles. For the cluster we choose (rather arbitrarily) one atom surrounded by 12 atoms of the same kind situated on an f.c.c. lattice. Finally, the HSPY structure factor, calculated within this model, is compared with our experimental diffraction data. We found that the two curves displayed hardly any resemblance. More particularly, we concluded from the calculated curves (which are not presented in this paper) that too much crystallinity had been incorporated in this model.

*4.2.4. HSPY including perturbation**

The hard-sphere solution of the Percus–Yevick equation for a binary system proves to give reasonable results for values of q close to the first peak. Because of the neglect of the long range interaction between the atoms in the liquid, the hard-sphere model fails to describe properly the long-wavelength limit of the partial structure factors. A number of authors [37, 39–42] suggest to use a weak long range potential $\phi_{ij}^{lr}(r)$ as a perturbation on the hard sphere system:

$$\phi_{ij}(r) = \phi_{ij}^{HS}(r) + \phi_{ij}^{lr}(r). \tag{4.3}$$

* *Note added in proof*: See also a recent paper by V. K. Ratti and A. B. Bhatia, Nuovo Cim. 43B (1978) 1.

The direct correlation function $c_{ij}(r)$ for larger r is given asymptotically by

$$c_{ij}(r) = -\phi_{ij}(r)/k_B T. \tag{4.4}$$

By substitution of eq. (4.3) into eq. (4.4), the long range as well as the short range effects of the potential on the direct correlation function are incorporated:

$$c_{ij}(r) = c_{ij}^{HS}(r) - \phi_{ij}^{lr}(r)/k_B T. \tag{4.5}$$

To avoid spurious oscillations in $c_{ij}(q)$ the perturbation potential should be continuous and following Bhatia [42] we change $\phi_{ij}^{lr}(r)$ into

$$\begin{aligned} \phi_{ij}^{lr}(r) &= \phi_{ij}^{lr}(d_{ij}), \quad r \leqslant d_{ij} \\ &= \phi_{ij}^{lr}(r), \quad r > d_{ij}, \end{aligned} \tag{4.6}$$

where d_{ij} is the value of r at which $\phi_{ij}^{lr}(r)$ has a minimum. Still adopting the suggestions of Ratti and Bhatia [37], we take

$$\phi_{ij}^{lr}(r) = A_{ij} \frac{d_{ij}}{r} \cdot e^{-(r-d_{ij})/d_{ij}}. \tag{4.7}$$

After some algebra, taking the Fourier transform of eq. (4.5):

$$c_{ij}(q) = c_{ij}^{HS}(q) - \frac{4\pi}{q^3} \cdot \frac{A_{ij}}{k_B T} \left[\sin u - u \cos u + \frac{u^2(\sin u + u \cos u)}{1 + u^2} \right], \tag{4.8}$$

where $u = q\, d_{ij}$. The partial structure factors are obtained by means of the Pearson–Rushbrooke relations [43].

Ratti and Bhatia [37] simply put $\phi_{11}^{lr}(r) = \phi_{22}^{lr}(r) = 0$, considering only the effect of $\phi_{12}^{lr}(r)$. This simplification implies that the HSPY structure factors of the pure components are unperturbed. We substitute $\eta = 0.45$, $d_{Na} = 3.15$ Å and $d_{Cs} = 4.80$ Å in accordance with our choice for the "straightforward" HSPY-method (section 4.2.1), while d_{NaCs} is set equal to $\frac{1}{2}(d_{Na} + d_{Cs})$. It was found by Ratti and Bhatia that, for $c_{Na} \approx 0.85$, $A_{NaCs}/k_B T = 0.0608$ gives the best fit of the theoretical $S(q)$ to the experimental $S(q)$;

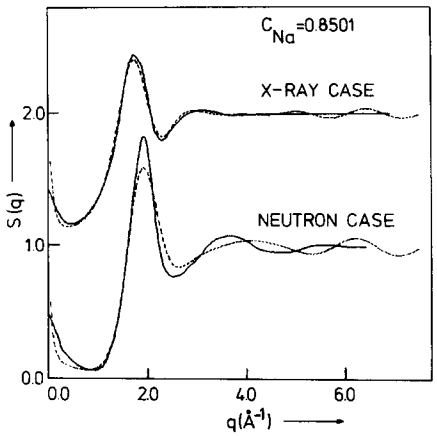

Fig. 23. Example of H.S.P.Y. results including Ratti–Bhatia correction (– – – –) compared with experimental values (———).

the results for this concentration are shown in fig. 23. We notice that this model accounts for the increase in $S(q)$ for decreasing small q-values. The positive value of A_{12} indicates that each atom is preferably surrounded by atoms of its own kind, which is consistent with our earlier findings.

4.3. Conformal solution theory

The conformal solution theory is based on the condition that, to good approximation, the pair potentials $\phi_{ij}(r)$ of the constituents in a binary liquid can be written as

$$\phi_{ij}(r) = A_{ij}\phi(\lambda_{ij}r), \tag{4.9}$$

where $\phi(r)$ is the pair potential of a (hypothetical) reference liquid. A_{ij} and λ_{ij} are constants deviating only slightly from unity. In this approximation, Parrinello et al. [44] derived a relation for $S_{CC}(q)$:

$$S_{CC}(q) = c(1-c) + \rho_0 c^2(1-c)^2\left(\frac{d_{12}}{k_B T}\right) \times \int_V \phi(r)g(r)\,e^{-iq\cdot r}dr, \tag{4.10}$$

where

$$d_{12} = 2A_{12} - A_{11} - A_{22}. \tag{4.11}$$

Taking potassium as reference liquid and using the results of the pair potential calculations carried out for the MD computer experiments (see next section), we have obtained numerical values of λ_{ij} and A_{ij} for two Na–Cs alloys, containing 60 and 85 at. % Na, respectively. We found that the A_{ij} may take values of about 2. This invalidates any application of the conformal solution theory. Furthermore, eq. (4.10) is symmetric with respect to the composition, in contrast with the experimental data. Further exploration of the conformal solution theory at its present stage seems therefore to be not meaningful.

4.4. Computer experiment in molecular dynamics (MD)

A technique which has been adapted to complement the description of the structure of liquid binary alloys by three partial structure factors is that of the computer experiment in molecular dynamics. In the present investigation, we have used the method of molecular dynamics (MD) to calculate the radial distribution functions of two Na–Cs alloys, with $c_{Na} = 0.60$ and $c_{Na} = 0.85$ at $T = 100°C$.

The interatomic potential is basic to any computer simulation of an array of atoms. It is well known that an exclusively pair-wise interatomic potential is not valid for describing the interaction between atoms of metals. Nevertheless, such potentials have been used frequently in computer simulation studies supposing that the volume-dependent electronic contribution can be subsumed into pair-wise interaction functions. To a degree, all interatomic interaction functions are empirical. Even pseudopotential theory is based on some assumptions rationalized only by comparison with experimental data. The method of model potentials [45] is based on the information about the core potential and core wave functions which are derived from spectroscopic data. The experimental information is introduced at the most fundamental level in contradistinction to empirical potentials which are fitted to phonon spectra.

The basic idea of a pseudopotential is to replace the strong potential inside the core of an ion by a weaker potential which eliminates the bound core states but has the same energy eigenvalues for the valence states. The pseudopotential method has been extensively discussed by several authors [46] and for a comprehensive survey reference should be made to the review of Heine and Weaire [47].

In the present work, the effective interatomic potentials of the sodium–caesium alloys are calculated, within the framework of the pseudopotential approximation, from model potentials of the Heine–Abarenkov–Shaw type [48–50]. A concise description of this type of pair-potentials is given by Lee et al. [51].

One of the parameters required for the calculation of the total interionic interaction function is the effective valence Z^* appearing in model potential theory. In order to obtain a concentration dependent potential for an alloy we take $\bar{Z}^*$ equal to $\Sigma_i c_i Z_i^*$ where c_i represents the concentration of the ith kind of atoms. In that way the Na–Na and Cs–Cs interactions are not the same in the alloys as in the pure metals. Another parameter involved is the model potential well $A_l(E)$ and its variation with energy at the Fermi level E_F for all l values. The Fermi momentum k_F depends on the mean atomic volume $\bar{\Omega}$. To a first approximation, we take $\bar{\Omega}$ equal to $\Sigma_i c_i \Omega_i$.

In fig. 24 the interionic potentials for the $Na_{85}Cs_{15}$ system are depicted. A Born–Mayer repulsive term [52, 53] representing the hard core, is included. The potentials are cut off at 8.94 Å, 10.42 Å and 11.27 Å for Na–Na, Na–Cs and Cs–Cs, respectively. In a similar plot (fig. 25) of the interionic potentials of $Na_{60}Cs_{40}$ the cut-off values are, in the same order, 9.26 Å, 11.21 Å and 12.33 Å. The composition dependence of the potentials is evident.

The first step in the computer simulation study is the construction of a large computational block of interacting atoms. The atoms are first randomly arranged in a cubical box and suitable periodic boundary conditions are imposed to eliminate the effects arising from a surface. Once these initial atomic positions have been determined, it is assumed that they will relax under the influence of the pairwise central forces which the atoms exert on each other. The forces are calculated from the interaction potentials. For determining the displacements from the initial to the final positions the equations of motions resulting from Newtonian mechanics are solved.

Given a number of atomic points (N), each with three degrees of freedom, determination of the velocities and positions of each atom would require an integration of $3N$ coupled differential equations. The uncertainties associated with the potential interaction functions used and the inconvenience of such a calcu-

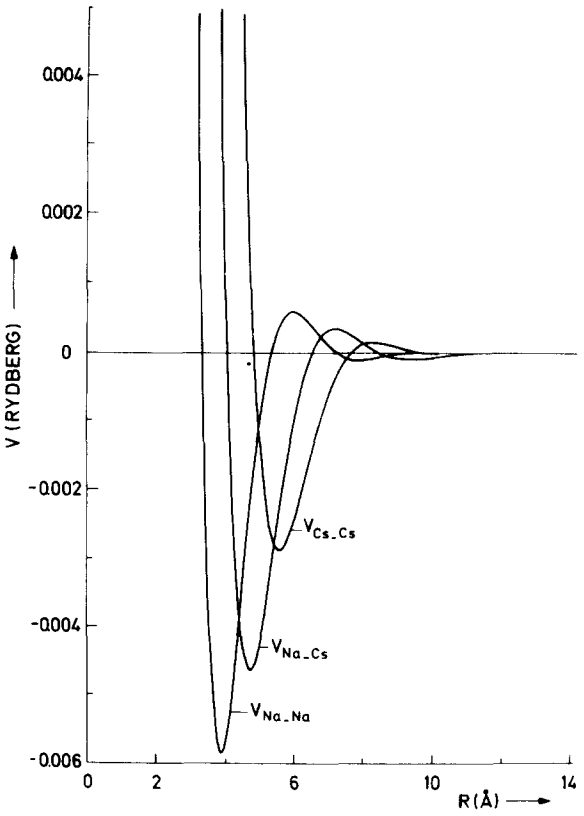

Fig. 24. Interionic pair potentials $V(R)$ for a Na–Cs alloy with composition $Na_{85}Cs_{15}$.

lation as regards computer time suggest that a simple difference procedure would give sufficient accuracy and would permit solutions to be obtained within a reasonable amount of computer time. The integration procedure of Rahman [54] is applied. In this so-called predictor-corrector method the time step Δt should be chosen small in comparison with the period of the oscillator in the Debye approximation. This condition excludes values of $\Delta t > 10^{-14}$ s. A further check on the Δt value chosen is furnished by repeating calculations with different values of Δt. We found that for $\Delta t < 10^{-14}$ s the results were consistent. Accordingly, $\Delta t = 5 \times 10^{-15}$ s was chosen in the calculations.

The dynamics of the lattice was studied under a constant volume condition. Therefore, the pressure in the lattice may be expected to increase with increasing temperature so that the motion of the atoms under study must be due to the combined effects of pressure and temperature. The effect of pressure was

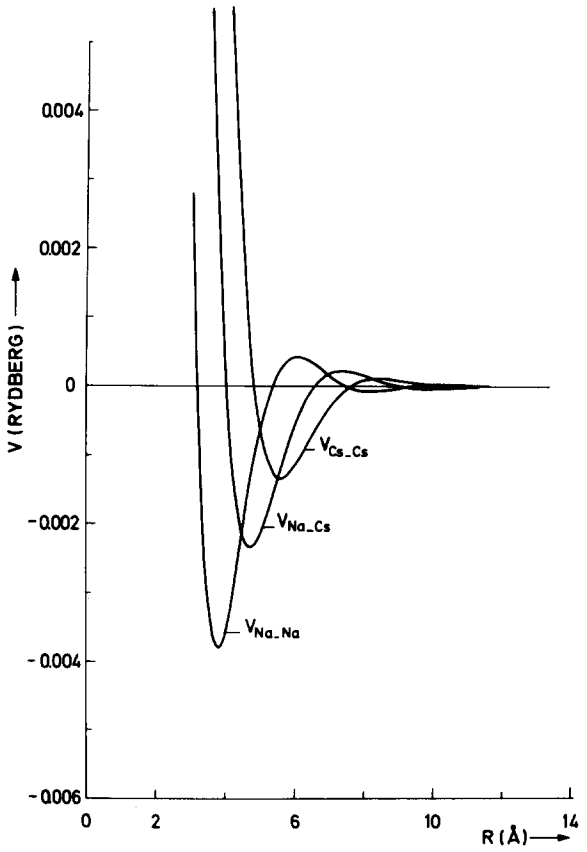

Fig. 25. Interionic pair potentials $V(R)$ for a Na–Cs alloy with composition $Na_{60}Cs_{40}$.

not separately studied in our calculations. The simulation of the temperature of the lattice is based on the conditions for thermal equilibrium in a classical system of coupled oscillators, i.e. (i) the total energy of the system is constant, (ii) the mean kinetic energy of the system is equipartitioned among the three degrees of freedom and (iii) the velocity distribution of the oscillators is Maxwellian. Since the anharmonicity of the alloys considered might be large, equipartition may not apply to the potential energies (see fig. 25). Consequently, the temperature of the lattice was obtained from its mean kinetic energy.

To speed up the relaxation procedure the method of Bullough and Perrin [55] is utilized where the configuration is periodically "quenched", i.e. halted when the kinetic energy attains a maximum. That method ensures very rapid convergence to the absolute minimum in total potential energy. An additional advantage of this method over the static method of Girifalco [56] is that one usually proceeds automatically past metastable intermediate stages and the true stable configuration can be obtained quickly. However, as the computational method is performed with finite time steps, it would be fortunate if one step $t + \Delta t$ would coincide exactly with the point in maximum kinetic energy. So several steps of freezing the atoms are necessary when the kinetic energy of the system reaches a maximum value.

It took about 250 time steps Δt to reach equilibrium for the $Na_{60}Cs_{40}$ and $Na_{85}Cs_{15}$ systems. The number of particles in the computational block is 216 for $c_{Na} = 0.60$ and 1728 for $c_{Na} = 0.85$. In both systems the averaged temperatures are 100°C. The oscillations of the temperature are about 15 K and 10 K, respectively. In fig. 26 the atomic configuration of a model Na–Cs (85% Na) liquid is depicted. Only one slice of atoms, with thickness of a sodium atom, is shown. It illustrates the clustering of Na and Cs atoms.

After the equilibrium configurations have been obtained for the $Na_{60}Cs_{40}$ and $Na_{85}Cs_{15}$ systems, we have run 2000 time steps Δt more in order to obtain

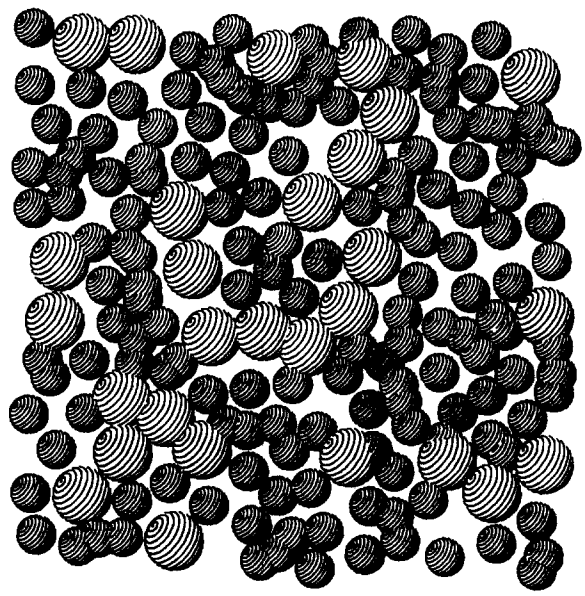

Fig. 26. Slice from a model $Na_{0.85}Cs_{0.15}$ liquid generated by computer simulation. The thickness of the slice is that of one sodium atom. The larger spheres are caesium atoms, which exhibit a tendency to clustering together.

the radial distribution functions $g_{ij}(r)$. The partial radial distribution functions obtained are shown in figs. 27 and 28 for the two compositions considered. It is noteworthy that going from $g_{11}(r)$ via $g_{12}(r)$ to $g_{22}(r)$ the height of the first peak decreases generally whereas the width increases correspondingly ($g_{22}(r)$ for 85% Na is perhaps an exception). This means that Na atoms being nearest neighbours of a Na atom have much better defined positions than Cs atoms being nearest neighbours of a Cs-atom.

The comparison between the MD results and the experimentally measured total interference functions can be done in two ways.

a) From the relation between $S(q)$ and $g_{ij}(r)$ (eq. 1.1) we can define a function $G(r)$, obeying the equations (4.12). In the case of X-rays, the Warren–Krutter–Morningstar (WKM) approximation [10] has to be used in the derivation of (4.12).

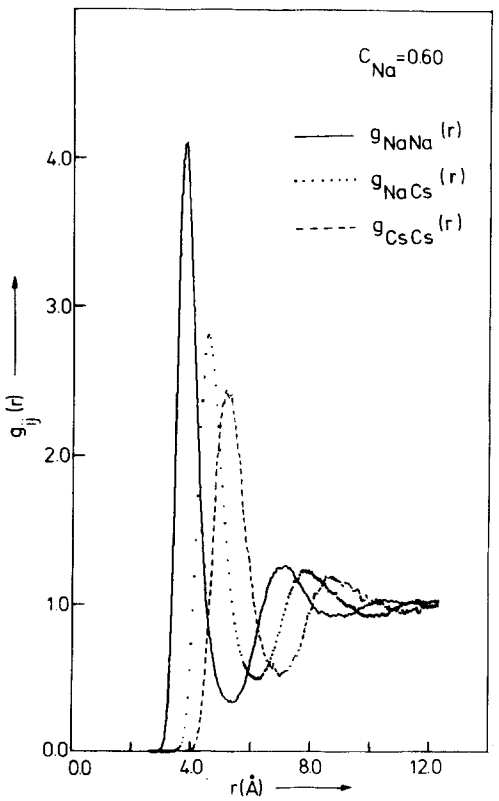

Fig. 27. Partial radial distribution functions $g_{ij}(r)$ obtained by MD computer simulation, for an alloy containing 60% sodium.

$$G(r) = 1 + \frac{1}{2\pi^2\rho_0 r}\int_0^\infty [S(q) - 1]\, q \sin qr\, dq$$

$$= c_1^2 \frac{f_1^2(q)}{\langle f_1^2(q)\rangle} g_{11}(r) + c_2^2 \frac{f_2^2(q)}{\langle f_2^2(q)\rangle} g_{22}(r)$$

$$+ 2c_1c_2 \frac{f_1(q)f_2(q)}{\langle f^2(q)\rangle} g_{12}(r) + \frac{\langle f^2(q)\rangle - \langle f(q)\rangle^2}{\langle f^2(q)\rangle}. \qquad (4.12)$$

When $S(q)$ is determined by neutron scattering, eq. (4.12) is exact since for this case the scattering lengths are independent of q. When $S(q)$ is obtained from X-ray scattering, eq. (4.12) is approximate. In that case the coefficients in front of $g_{ij}(r)$ are calculated for the wavenumber for which $S(q)$ attains its main maximum.

The results for $G(r)$ as calculated from X-ray and neutron diffraction data are plotted in figs. 29 and 30 for 60 and 85% Na, together with the M.D. results obtained for $G(r)$. The agreement between the two curves in each figure is good as far as the *positions* of the maxima and minima in $G(r)$ are concerned, but the agreement is less satisfactory if one considers the *values* of $G(r)$ at these maxima.

b) Going the other way around one can calculate the F.Z. partial structure factors by Fourier transformation of $g_{ij}(r)$ and, subsequently, calculate $S(q)$. This procedure has the disadvantage that, as a consequence of the necessary cut-off, the $g_{ij}(r)$ as calculated by MD, include a smaller number of oscillations than the $S(q)$ obtained experimentally. This cut-off results in spurious oscillations at small wavenumbers in the Fourier transforms of $g_{ij}(r) - 1$. The $S(q)$, obtained in this way for $c_{Na} = 0.60$ and $c_{Na} = 0.85$, are depicted in figs. 31a and b and they are compared with our experimental data. We notice, once more, that the *positions* of the maxima and minima agree rather well, whereas the *values* of $S(q)$ at those wavenumbers differ strongly, particularly for $c_{Na} = 0.85$. Like for $G(r)$, the MD calculations result in exaggerated oscillations of $S(q)$.

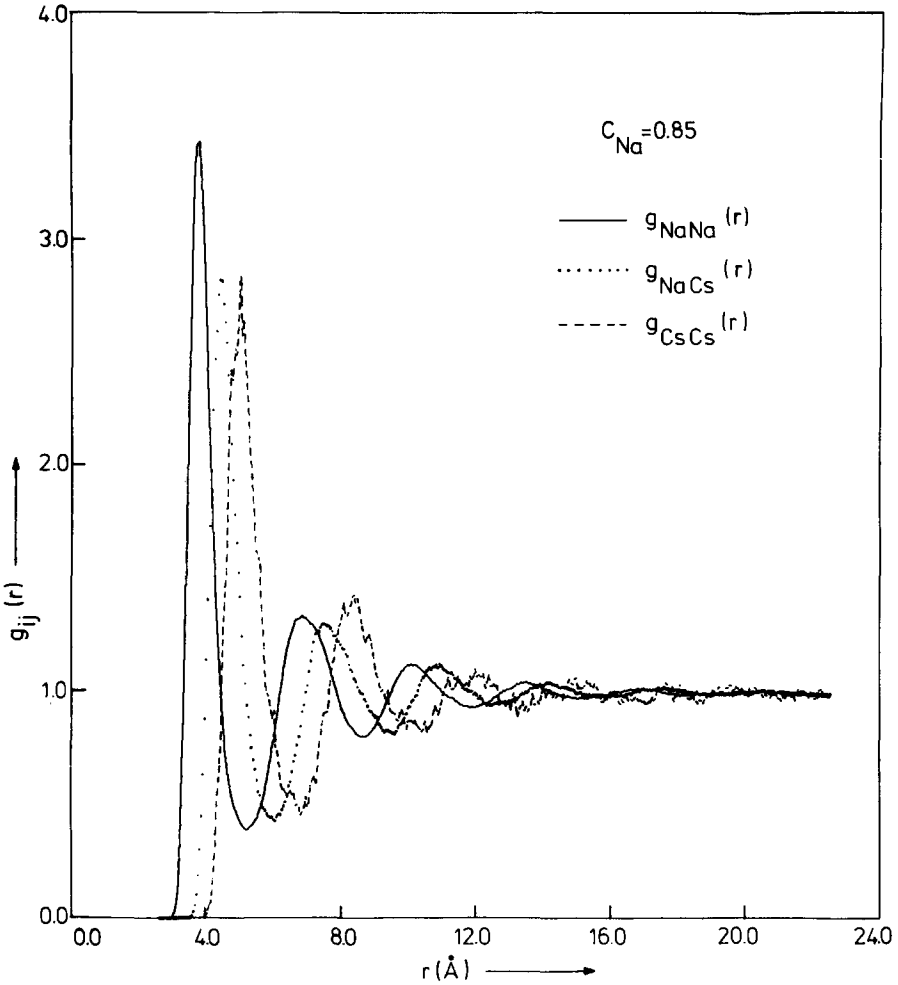

Fig. 28. Partial radial distribution functions $g_{ij}(r)$ obtained by MD computer simulation, for an alloy containing 85% sodium.

4.5. Partial structure factors for three sodium–caesium alloys

In the preceding sections we have considered several models for interpreting the experimental data. In the following we will, for three concentrations, with 30, 60 and 85 at. % Na respectively, compare the partial structure factors deriving from the different approaches and discuss the most favourable ones for each interval of wave vectors.

To start with, the approximation of composition independent FZ partial structure factors (section 4.1) is disqualified. The main reason for doing so is its failure, for some concentrations, to describe properly the $S(q)$ from $q = 0$ up to the first peak (fig. 17). Another reason will be mentioned below. The model based on "molecular clusters" is rejected because it fails completely to reproduce the experimental $S(q)$ for neutron as well as X-ray scattering.

4.5.1. $c_{Na} = 0.30$

For this composition two theoretical models are left to calculate the partial structure factors: the HSPY theory with fixed η and d_i and the HSPY theory in which η and d_i are q-dependent in the way as explained above. For either of the two approxi-

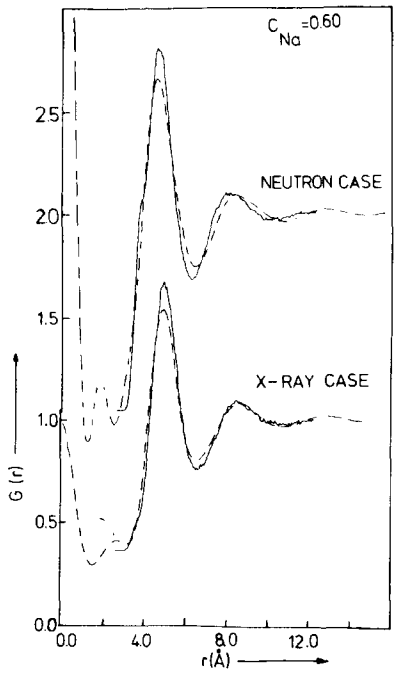

Fig. 29. $G(r)$ (defined in eq. (4.12)) for an alloy containing 60% Na. – – – – – by Fourier transformation of experimental $S(q)$; ——— from MD calculations.

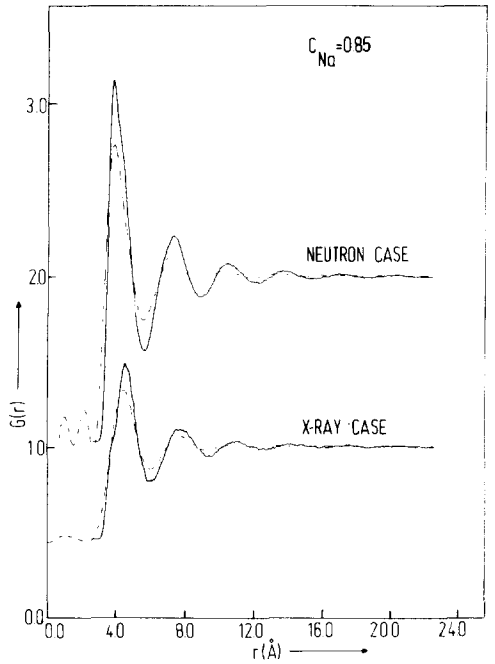

Fig. 30. $G(r)$, defined in eq. (4.12), for an alloy containing 85% Na. – – – – – by Fourier transformation of experimental $S(q)$; ——— from MD calculations.

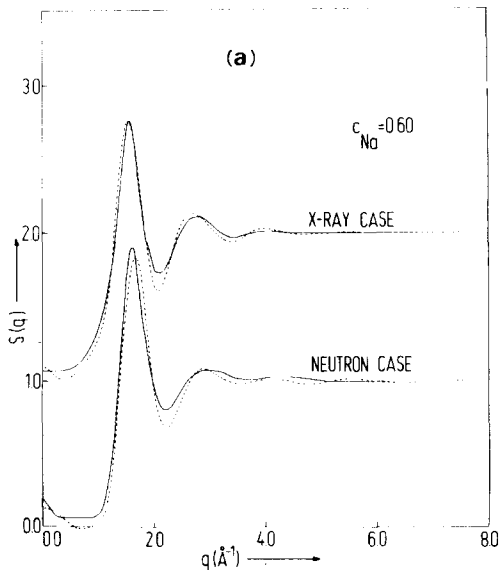

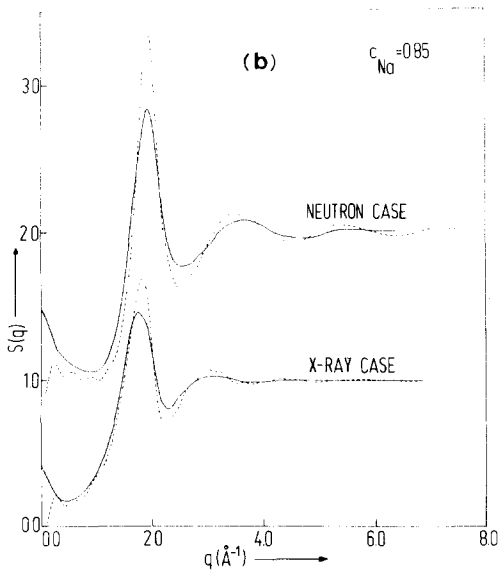

Fig. 31a, b. Experimental $S(q)$ (———) compared with $S(q)$ obtained from MD $g_{ij}(r)$ by Fourier transformation (– – – – –). Results are given for X-ray as well as neutron diffraction. (a) Alloy with 60% sodium; (b) alloy with 85% sodium.

mations we have depicted the three partial structure factors $S_{ij}(q)$ in fig. 32, and we see that there exists a satisfactory overall agreement. Indeed, for all three partial structure factors, the curves with fixed η and d_i exhibit the larger oscillation amplitude for large values of q. This phenomenon was already observed for the total interference function (cf. figs. 19 and 20).

Additionally, for $c_{Na} = 0.30$, $S_{CsCs}(q)$ and $S_{NaCs}(q)$ may be obtained more directly from experiment, using the following arguments. From fig. 32 we notice that the amplitude of the oscillations of the Na–Na partial structure factor is much smaller than that of the other partial structure factors. The value of $S_{NaNa}(q)$ never deviates strongly from 1. Taking into account that for $c_{Na} = 0.30$ this component gives only a minor contribution to the X-ray as well as to the neutron total interference function (which can be deduced from e.g. fig. 13), we may approximate $S_{NaNa}(q)$ by the value 1 for all values of q. Then, $S_{CsCs}(q)$ and $S_{NaCs}(q)$ can be calculated from the experimental X-ray and neutron total interference functions. These results will be referred to as "semi-experimental"; they are also included in fig. 32. We notice that $S_{CsCs}(q)$, obtained from this approximation, is similar to the corresponding curves from both hard-sphere models. $S_{NaCs}(q)$, however, shows some deviations from the hard-sphere ones. Closer inspection shows that these discrepancies are not the result of the approximation $S_{NaNa}(q) = 1$. Discrepancies with the HSPY results also occur for small values of q of $S_{NaCs}(q)$ and $S_{CsCs}(q)$. It can be shown, that the HSPY value for $S_{CsCs}(0)$ is outside the limits of error of the "semi-experimental" value for it.

4.5.2. $c_{Na} = 0.60$

For this composition, three sets of partial structure factors are considered; besides the two hard-sphere models, mentioned above, MD calculations for $g_{ij}(r)$ are available for deriving a third set of partial structure factors. All three sets are shown in fig. 33. Like for $c_{Na} = 0.30$ we notice that $S_{CsCs}(q)$ exhibits approximately the same behaviour in all three models. The agreement between the different $S_{NaCs}(q)$ results is slightly worse. The dip in the MD results for small q-values in $S_{CsCs}(q)$ and $S_{NaCs}(q)$ arises from spurious oscillations introduced by the Fourier transformations of the computer results for $g_{ij}(r)$.

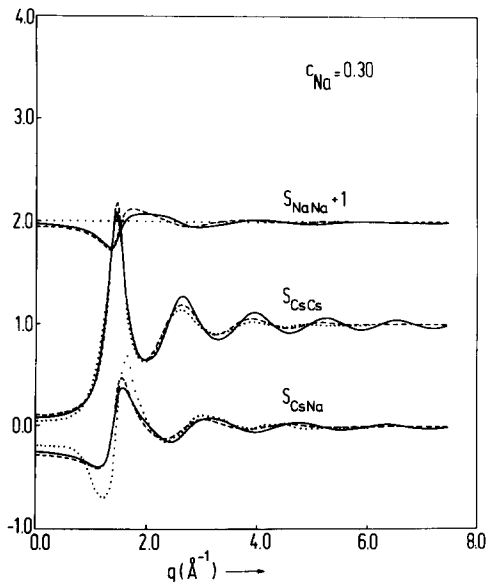

Fig. 32. AL partial structure factors obtained from different models for an alloy with 30% sodium: ——— HSPY (fixed η, d_i); – – – – – HSPY (variable η, d_i); · · · · · "semi-experimental" structure factors.

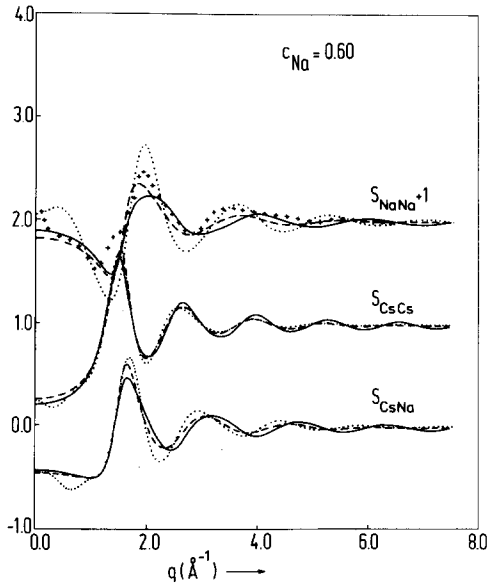

Fig. 33. AL partial structure factors obtained from different models for an alloy with 60% sodium: ——— HSPY (fixed η, d_i); – – – – – HSPY (variable η, d_i); · · · · · computer simulation; +++++ "semi-experimental", from neutron data.

On the contrary, a strongly diverging set of curves for $S_{NaNa}(q)$ is found. Particularly the large oscillation amplitude of the MD data is remarkable. Because of the discrepancy among the $S_{NaNa}(q)$ data (for the two HSPY models this may be due to the strong η-dependence of the partial structure factor for the component with the smaller hard-sphere radius), we have performed the following calculation to obtain a reasonable guess at $S_{NaNa}(q)$. Starting from the observation that the curves for $S_{CsCs}(q)$ and $S_{NaCs}(q)$ seem to be quite well described by the HSPY theory with variable η and d_i, we can calculate $S_{NaNa}(q)$ with reasonable accuracy from the neutron total interference function. These results for $S_{NaNa}(q)$ are included in fig. 33. They will be denoted as the "semi-experimental" values for this concentration. Some discrepancies between this and the other curves are noteworthy. Particularly, the dip in front of the first peak is shifted towards smaller q-values. It is not possible to apply this method to the X-ray scattering results. This is a consequence of the Na–Na term giving only a minor contribution to the X-ray total interference function.

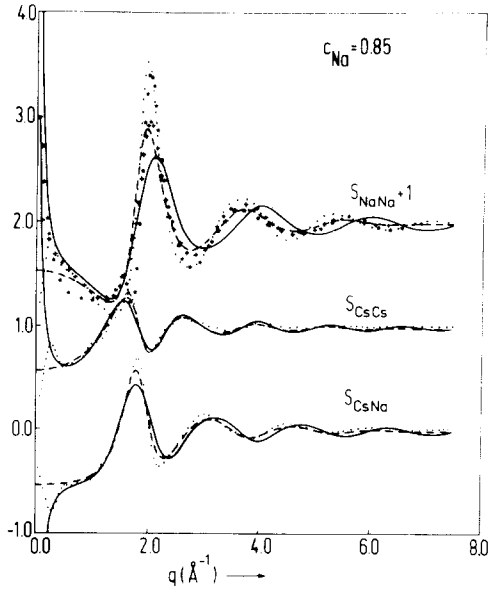

Fig. 34. AL partial structure factors obtained from different models for an alloy with 85% sodium: ——— HSPY (fixed η, d_i); – – – – – HSPY (variable η, d_i); · · · · · computer simulation; +++++ "semi-experimental", from neutron data; ***** "semi-experimental", from X-ray data.

4.5.3. $c_{Na} = 0.85$

Three sets of partial structure factors, obtained by the same procedures as for $c_{Na} = 0.60$, are considered. They are shown in fig. 34. For this alloy composition, the Ratti–Bhatia correction is included in the HSPY model with fixed η and d_i. As a consequence, the partial structure factors show a steep rise for q approaching zero. The MD results exhibit some spurious oscillations. Once more, reasonable agreement exists between the various results for $S_{NaCs}(q)$ and $S_{CsCs}(q)$, whereas the $S_{NaNa}(q)$ results differ considerably among themselves. Therefore, like for $c_{Na} = 0.60$, S_{NaCs} and S_{CsCs} seem to be described satisfactorily by the HSPY model with variable η and d_i and "semi-experimental" values of $S_{NaNa}(q)$ can be calculated from the X-ray as well as from the neutron diffraction data. Both results are included in fig. 34 and both agree well with the HSPY theory with variable η and d_i as well as with the MD results. For $q < 1.5$ Å^{-1}, $S_{NaNa}(q)$ as derived from the neutron experiments follows almost exactly the HSPY data with fixed η and d_i, in contrast with the X-ray results for $S_{NaNa}(q)$. Indeed, $S_{NaNa}(q)$ appears to give a much larger contribution to the neutron intensities than to the X-ray intensities.

4.5.4. Concluding remarks

When comparing figs. 32, 33 and 34 we notice that the positions of the main peaks of the $S_{ij}(q)$ are not independent of the composition. This is an additional argument for discarding the approximation of concentration independent FZ structure factors.

Furthermore, we notice that, as expected, the Ratti–Bhatia version of the HSPY model accounts qualitatively for the rise of the long-wavelength limit of the partial structure factors due to concentration fluctuations. But quantitatively, discrepancies up to a factor of 2 remain when the results are compared with the thermodynamic values of $S(0)$.

We have, for want of anything better, chosen for an opportunist approach to the problem of establishing partial structure factors of Na–Cs mixtures, adapting our analysis to the particular alloy compositions and ranges of q. Nevertheless, the uncertainties in the partial structure factors derived are so large, that we can hardly recommend a special set as being most favourite.

The definitive determination still waits for a more fundamental approach to the understanding of typically non-ideal mixtures, of which the liquid Na–Cs system is an example.

Acknowledgements

The authors acknowledge with thanks the contributions of Dr. T. Lee and J. Bisschop to the initial stage of the MD computer simulation experiment. H. van Hasselt and K. van der Weg assisted during some of the diffraction experiments. J. Numan, F. van der Horst and G. J. B. Vinke provided technical assistance.

This work forms part of the research program of the "Stichting voor Fundamenteel Onderzoek der Materie" (Foundation for Fundamental Research of Matter – FOM) and was made possible by financial support from the "Nederlandse Organisatie voor Zuiver-Wetenschappelijk Onder zoek" (Netherlands Organization for the Advancement of Pure Research – ZWO).

References

[1] M. J. Huijben, H. Klaucke, J. Hennephof and W. van der Lugt, Scr. Met. 9 (1975) 653.
[2] P. D. Feitsma, J. Hennephof and W. van der Lugt, Phys. Rev. Letters 32 (1974) 295.
[3] P. D. Feitsma, J. J. Hallers, W. van der Lugt and T. Lee, Physica 93B (1978) 47.
[4] M. G. Kim and S. V. Letcher, J. Chem. Phys. 55 (1971) 1164.
[5] K. Ichikawa, S. M. Grannstaff, Jr. and J. C. Thompson, J. Chem. Phys. 61 (1974) 4059.
[6] N. W. Ashcroft and D. C. Langreth, Phys. Rev. 156 (1967) 685.
[7] A. B. Bhatia and D. E. Thornton, Phys. Rev. B2 (1970) 3004.
[8] T. E. Faber and J. M. Ziman, Phil. Mag. 11 (1965) 153.
[9] M. J. Huijben and W. van der Lugt, Acta Cryst. A35 (1979) 431.
[10] B. E. Warren, H. Krutter and O. Morningstar, J. Am. Ceram. Soc. 19 (1936) 202.
[11] Neutron Cross Section Data, C. G. Shull, ed., Compilation M.I.T. (1971).
[12] M. J. Huijben, T. Lee, W. Reimert and W. van der Lugt, J. Phys. F: Metal Phys. 7 (1977) L119.
[13] H. C. Reimsch, Smoothing by Spline Functions, Numerische Mathematik 10 (1967) 177.
[14] A. Guinier, Ann. Phys. 12 (1939) 161.
[15] A. B. Bhatia and N. H. March, J. Phys. F: Metal Phys. 5 (1975) 1100.
[16] P. J. Flory, J. Chem. Phys. 10 (1942) 51.
[17] T. Yokokawa and O. J. Kleppa, J. Chem. Phys. 40 (1964) 46.
[18] B. J. McClelland, Statistical Thermodynamics (Chapman and Hall, London, 1973).
[19] K. Ichikawa and J. C. Thompson, J. Phys. F: Metal Phys. 4 (1974) L9.
[20] R. Hezel and S. Steeb, Z. Naturforsch. 25a (1970) 1085.
[21] J. Hoehler and S. Steeb, Z. Naturforsch. 30a (1975) 775.
[22] W. Zaiss and S. Steeb, Phys. Chem. Liq. 6 (1976) 21.
[23] Y. Waseda and M. Ohtani, Phys. Stat. Sol. (b) 48 (1971) K77.
[24] H. F. Bühner and S. Steeb, Z. Naturforsch. 24a (1969) 428.
[25] H. F. Bühner and S. Steeb, Z. Metallk. 62 (1971) 27.
[26] H. F. Bühner and S. Steeb, Z. Naturforsch. 25a (1970) 1862.
[27] W. Knoll and S. Steeb, Phys. Chem. Liquids 4 (1973) 27.
[28] W. E. Lukens and C. N. J. Wagner, Z. Naturforsch. 30a (1975) 242.
[29] W. E. Lukens and C. N. J. Wagner, Z. Naturforsch. 28a (1973) 297.
[30] N. C. Halder, D. M. North and C. N. J. Wagner, Phys. Rev. 177 (1969) 47.
[31] C. N. J. Wagner, N. C. Halder and D. M. North, Z. Naturforsch. 24a (1969) 432.
[32] B. R. Orton and S. P. Woodisse, J. Phys. F: Metal Phys. 4 (1974) 2103.
[33] V. I. Korsunsky and Yu. I. Naberukhin, Phys. Chem. Liq. 5 (1976) 137.
[34] J. L. Lebowitz, Phys. Rev. 133 (1964) A895.
[35] A. J. Greenfield, N. Wiser, M. R. Leenstra and W. van der Lugt, Physica 59 (1972) 571.
[36] J. Hafner, Phys. Rev. A16 (1977) 351.
[37] V. K. Ratti and A. B. Bhatia, private communication.
[38] A. B. Bhatia and V. K. Ratti, J. Phys. F: Metal Phys. 6 (1976) 927.
[39] J. Woodhead-Galloway, T. Gaskell and N. H. March, J. Phys. C: Sol. State Phys. 1 (1968) 271.
[40] J. Woodhead-Galloway and T. Gaskell, J. Phys. C: Sol. State Phys. 1 (1968) 1472.
[41] T. Gaskell, J. Phys. C: Sol. State Phys. 3 (1970) 240.
[42] A. B. Bhatia, Inst. Phys. Conf. Ser. No. 30, pp. 21–38 (1977) London.
[43] F. J. Pearson and G. S. Rushbrooke, Proc. Roy. Soc. Edinb. A64 (1957) 305.
[44] M. Parrinello, M. P. Tosi and N. H. March, Proc. Roy. Soc. London A341 (1974) 91.
[45] V. Heine and I. Abarenkov, Phil. Mag. 9 (1964) 451.
[46] W. A. Harrison, Pseudopotentials in the Theory of Metals (Benjamin, Reading, 1966) p. 5.
[47] V. Heine and D. Weaire, Solid State Physics (H. Ehrenreich, F. Seitz and D. Turnbull, eds.) (Academic Press, London, 1970) Vol. 24, p. 249.
[48] R. W. Shaw, Phys. Rev. 174 (1968) 769.

[49] M. Appapillai and A. R. Williams, J. Phys. F: Metal Phys. 3 (1973) 759.
[50] J. J. Hallers, T. Mariën and W. van der Lugt, Physica 78 (1974) 259.
[51] T. Lee, J. Bisschop, W. van der Lugt and W. F. van Gunsteren, Physica 93 (1978) 59.
[52] A. A. Abrahamson, Phys. Rev. 178 (1969) 76.
[53] W. Cochran, Proc. Roy. Soc. (London) A276 (1963) 368.
[54] A. Rahman, Phys. Rev. 136 (1964) A405.
[55] A. Bullough and R. C. Perrin, Proc. Roy. Soc. (London) A305 (1968) 541.
[56] L. A. Girifalco and V. G. Wizer, J. Phys. Chem. Solids 12 (1960) 260.
[57] P. A. Doyle and P. S. Turner, Acta Cryst. A24 (1968) 390.
[58] D. T. Cromer and D. Liberman, J. Chem. Phys. 53 (1970) 1891.